

Interplay between local and global order controls bifurcations in nonreciprocal systems without a conservation law

Kristian Blom,¹ Uwe Thiele,^{2,3,4} and Aljaž Godec^{1,*}

¹*Mathematical bioPhysics group, Max Planck Institute for Multidisciplinary Sciences, Göttingen 37077, Germany*

²*Institute of Theoretical Physics, University of Münster, Münster 48149, Germany*

³*Center for Nonlinear Science (CeNoS), University of Münster, Münster 48149, Germany*

⁴*Center for Multiscale Theory and Computation (CMTC),*

University of Münster, Münster 48149, Germany

(Dated: July 31, 2024)

We elucidate the generic bifurcation behavior of local and global order in short-range interacting nonreciprocal lattice systems without conservation laws. We show that a critical magnitude of nearest-neighbor correlations within the respective lattices controls the emergence of coherent oscillations of global order as a result of frustration. Local order is maintained during these oscillations, implying non-trivial spatio-temporal correlations. Ghost states emerge in the strong-interaction regime. The residence time in either of these states eventually diverges, giving rise to ordered non-equilibrium steady states via a saddle-node-infinite-period bifurcation. Our work provides a comprehensive microscopic understanding of collective phenomena in nonreciprocal matter without conservation laws, which may be relevant e.g. for understanding enzyme clustering.

The last decade saw a surge of interest in multicomponent systems with nonreciprocal interactions. Nonreciprocity is commonly found in active and non-equilibrium systems [1–5], such as non-equilibrium fluids [6], predator-prey [7, 8] and many-body lattice [9–14] systems, spin glasses [15–17], active solids with odd elasticity [18], cell-cell interactions [19], optically trapped nanoparticles [20, 21], complex plasma dynamics [22–24], mixtures of passive and active particles [25] as well as chemically active interacting particles [26–29], primitive metabolic cycles [30], quorum-sensing active particles [31], and non-Hermitian quantum systems [32–34]. The importance of nonreciprocal interactions is meanwhile also widely recognized in the social sciences [35, 36], neuroscience [37, 38], and robotics [39].

At the microscopic level, nonreciprocal interactions are closely linked to the violation of Newton’s third law and broken detailed-balance [2, 22]. On the collective level, nonreciprocally interacting systems can resist coarsening and instead self-organize into dynamic states with unique temporal and spatial patterns, including traveling and oscillatory states [40–47]. Phenomenologically, such systems are typically described by a nonvariational coupling of Cahn-Hilliard models or Allen-Cahn models (i.e., the respective models B and A in [48]).

An important aspect of nonreciprocal systems is the presence of conservation laws. In the case of two nonvariational coupled fields one may have no [9, 17, 49, 50], one [51–53], or two [2, 25, 41, 42, 44, 47, 54] conservation laws. Nonreciprocal systems without conservation laws are particularly relevant in the realm of chemical reaction networks, where it was shown that kinetic asymmetries between enzymes may lead to nonreciprocal interactions [29].

There is growing interest in a bottom-up understanding of non-conserved nonreciprocal systems, so far limited to phenomenological and mean-field theory [9, 17, 49]. These works revealed intriguing phenomena, such as large-scale Hopf instabilities [9, 17, 49], saddle-node bifurcations [49, 50], and hidden collective oscillations [17]. However, a microscopic understanding of the bifurcation behavior remains elusive.

Here, we go beyond mean-field reasoning and develop a thermodynamically consistent description of nonreciprocal binary systems without conservation laws, starting from a pair of coupled Ising models. We incorporate nearest-neighbor correlations and consider both, *global and local order*. We explain why a critical magnitude of nearest-neighbor correlations controls the symmetry-breaking transition in the long-range order, in turn bounding the onset of coherent oscillations. We elucidate how the bifurcation behavior depends on interparticle interactions, and highlight stark differences in the spatio-temporal dynamics of all-to-all (mean-field) versus short-range-interacting systems; the square and Bethe lattices display equivalent behavior that is strikingly different from the all-to-all lattice. Our work provides a deeper microscopic understanding of collective phenomena in nonreciprocal matter with more realistic short-ranged interactions.

Fundamentals.—Consider a pair of lattices denoted by $\mu = a, b$, as shown in Fig. 1a, each having a coordination number z and periodic boundary conditions. On each lattice there are N spins that can assume two states $\sigma_i^\mu = \pm 1$, with $i \in \{1, \dots, N\}$ enumerating the spin’s location. Each spin interacts with its z nearest-neighbors on the same lattice and the spin at the equivalent position on the opposing lattice. The *local* interaction [55] energy of spin i on lattice μ can be written as (see also [49])

$$E_i^\mu = -J_\mu \sigma_i^\mu \sum_{\langle i|j \rangle} \sigma_j^\mu - K_\mu \sigma_i^a \sigma_i^b, \quad (1)$$

* agodec@mpinat.mpg.de

where $\langle i|j \rangle$ denotes a sum over nearest-neighbors j of spin i . Throughout, we will express energies in units of $k_B T$, where T is the temperature of the heat bath. The parameters J_μ and K_μ denote the coupling within lattice μ and of the spins in μ with those on the opposing lattice, respectively. When $K_a \neq K_b$, equivalent spins on the opposing lattices interact nonreciprocally.

We consider single spin-flip Glauber dynamics [57]. Let $P(\boldsymbol{\sigma}; t)$ be the probability at time t to find the system in state $\boldsymbol{\sigma} = \{\sigma_1^a, \sigma_1^b, \dots, \sigma_N^a, \sigma_N^b\}$ which is governed by the master equation $dP(\boldsymbol{\sigma}; t)/dt = \sum_\mu \sum_i [w_i^\mu(-\sigma_i^\mu)P(\boldsymbol{\sigma}'_{\mu,i}; t) - w_i^\mu(\sigma_i^\mu)P(\boldsymbol{\sigma}; t)]$, where $\boldsymbol{\sigma}'_{\mu,i} = \{\sigma_1^a, \sigma_1^b, \dots, -\sigma_i^\mu, \dots, \sigma_N^a, \sigma_N^b\}$ is a state which differs from state $\boldsymbol{\sigma}$ by one spin flip. The transition rates $w_i^\mu(\sigma_i^\mu)$ to flip a spin $\sigma_i^\mu \rightarrow -\sigma_i^\mu$ are uniquely specified by limiting the interactions to nearest neighbors, imposing isotropy in position space, and requiring that for $K_a = K_b$ the transition rates obey detailed-balance. These physical restrictions then lead to the general result $w_i^\mu(\sigma_i^\mu) = [1 - \tanh(\Delta E_i^\mu/2)]/2\tau$ [9, 17, 49], where $\Delta E_i^\mu = -2E_i^\mu$ is the change in energy on the $\mu = a \vee b$ lattice after spin conversion $\sigma_i^\mu \rightarrow -\sigma_i^\mu$, and $\tau \equiv 2N$ is an intrinsic timescale for spin flips to occur.

We are interested in the temporal dynamics of global and local order parameters averaged over all spins. The magnetization or long-range order [58] is given by

$$m^\mu(t) \equiv \frac{1}{N} \sum_{i=1}^N \langle \sigma_i^\mu(t) \rangle, \quad (2)$$

where $\langle f(t) \rangle \equiv \sum_{\boldsymbol{\sigma}} P(\boldsymbol{\sigma}; t) f(\boldsymbol{\sigma})$. Note that $m^\mu(t) \in [-1, 1]$. The three short-range order parameters [58] are

$$q^{\mu\mu}(t) \equiv \frac{2}{zN} \sum_i \sum_{\langle i|j \rangle} \langle \sigma_i^\mu(t) \sigma_j^\mu(t) \rangle, \quad (3)$$

$$q^{ab}(t) \equiv \frac{1}{N} \sum_{i=1}^N \langle \sigma_i^a(t) \sigma_i^b(t) \rangle, \quad (4)$$

with correlations $C^{\mu\nu}(t) \equiv q^{\mu\nu}(t) - m^\mu(t)m^\nu(t)$. We distinguish between the short-range order within and between the lattices. The alignment of spin pairs within lattice μ is quantified by $q^{\mu\mu}(t)$, and $q^{ab}(t)$ measures the alignment of equivalent spins on opposing lattices. The normalization in Eq. (3) follows from the fact that $zN/2$ is the number of nearest neighbor pairs in a periodic lattice with coordination number z , which renders $q^{\mu\mu}(t), q^{ab}(t) \in [-1, 1]$.

Evolution equations.—Our first main result is an *exact* set of coupled differential equations for the order parameters in the thermodynamic limit $N \rightarrow \infty$, which reads (see [56] for a detailed derivation)

$$\begin{aligned} \tau \frac{dm^\mu(t)}{dt} + m^\mu(t) &= \sum_{l,n} \mathcal{P}_{l,n}^\mu(t) \tanh(U_{l,n}^\mu), \\ \tau \frac{dq^{\mu\mu}(t)}{dt} + 2q^{\mu\mu}(t) &= \frac{2}{z} \sum_{l,n} (2l-z) \mathcal{P}_{l,n}^\mu(t) \tanh(U_{l,n}^\mu), \\ \tau \frac{dq^{ab}(t)}{dt} + 2q^{ab}(t) &= \sum_\mu \sum_{l,n} (2n-1) \mathcal{P}_{l,n}^\mu(t) \tanh(U_{l,n}^\mu), \end{aligned} \quad (5)$$

where $\sum_{l,n} \equiv \sum_{l=0}^z \sum_{n=0}^l$ is a sum over all possible nearest neighbor spin values on the same ($l = 0, \dots, z$) and opposing ($n = 0, 1$) lattice, $U_{l,n}^\mu \equiv [2l-z]J_\mu + [2n-1]K_\mu$, and $\mathcal{P}_{l,n}^\mu(t) \in [0, 1]$ is the time-dependent probability to select an up or down spin which has l neighboring up spins on the same lattice, and n neighboring up spins on the opposing lattice. The probability is normalized as $\sum_{l,n} \mathcal{P}_{l,n}^\mu(t) = 1$. The equations (5) are not yet closed; evaluating $\mathcal{P}_{l,n}^\mu(t)$ for an arbitrary lattice is a daunting combinatorial task, since it depends on microscopic details and therefore on an infinite hierarchy of higher order parameters.

An accurate closed-form expression for $\mathcal{P}_{l,n}^\mu(t)$ can be obtained with the Bethe-Guggenheim (BG) approximation, where we assume perfect mixing of nearest neighbor spin pairs. Such an approximation is exact on loopless lattices like the Bethe lattice [59], or large random graphs with fixed coordination number [60, 61]. As we show below, the spatio-temporal dynamics on these lattices agrees with the behavior on the square lattice. Note that a theory of the nonreciprocal Ising model on the fully-connected mean-field lattice has been constructed in [49], which we also report in Appendix A.

We split $\mathcal{P}_{l,n}^\mu(t)$ in “up” and “down” spin contributions $\mathcal{P}_{l,n}^\mu(t) = \mathcal{P}_{l,n}^{\mu+}(t) + \mathcal{P}_{l,n}^{\mu-}(t)$, where, e.g., $\mathcal{P}_{l,n}^{\mu+}(t) \in [0, 1]$ is the probability of flipping an up spin with l up neighbors on the same and n up neighbors on the opposing lattice, respectively. These probabilities read [56] (omitting the explicit t -dependence on the r.h.s.)

$$\mathcal{P}_{l,n}^{\mu\pm}(t) = \frac{C_l^z (1 \pm 2m^a + q^{aa})^{\delta_l^\pm} (1 \pm m^a - m^b \mp q^{ab})^{1-n}}{(1 \pm m^a)^z (1 - q^{aa})^{-\delta_l^\mp} (1 \pm m^a + m^b \pm q^{ab})^{-n}}, \quad (6)$$

where $C_l^z \equiv \binom{z}{l}/2^{z+2}$, $\delta_l^+ = l$, and $\delta_l^- = z - l$. The expression for $\mathcal{P}_{l,n}^{\mu\pm}(t)$ follows from Eq. (6) by replacing $m^a \rightarrow m^b$ and $q^{aa} \rightarrow q^{bb}$. Inserting Eq. (6) into Eqs. (5) yields a closed system of five coupled nonlinear differential equations.

Linear stability analysis.—We focus on the symmetric nonreciprocal setting $J_a = J_b = J$ and $K_a = -K_b = K$, also known as the perfectly nonreciprocal [16] setting. We start with the linear stability analysis of Eqs. (5) around their steady state. The trivial steady state corresponds to the disordered state with $m_s^\mu = 0$, $q_s^{ab} = 0$, and $q_s^{\mu\mu} \equiv q_s(J, K) \neq 0$ which is explicitly given in [56]. Up to first order, small perturbations $\delta \mathbf{m}(t) \equiv (\delta m^a(t), \delta m^b(t))$ decouple from perturbations $\delta \mathbf{q}(t) \equiv (\delta q^{aa}(t), \delta q^{bb}(t), \delta q^{ab}(t))$, and we obtain the linear equation $\tau d\delta \mathbf{m}(t)/dt = \mathbf{M}(q_s; J, K) \delta \mathbf{m}(t)$ (see [56] for the linear equation for $\delta \mathbf{q}(t)$). The elements of the linear stability matrix, $M_{\mu\nu}(q_s; J, K)$, read

$$\begin{aligned} M_{aa} = M_{bb} &= \frac{q_s/q_{\text{crit}} - 1}{1 + q_s} [1 - 2 \sum_{l,n} \bar{\mathcal{P}}_l^+ \tanh(U_{l,n}^a)], \\ M_{ab} = -M_{ba} &= \sum_{l,n} (2n-1) [\bar{\mathcal{P}}_l^+ + \bar{\mathcal{P}}_l^-] \tanh(U_{l,n}^a), \end{aligned} \quad (7)$$

where $\bar{\mathcal{P}}_l^\pm(q_s) \equiv C_l^z (1 \mp q_s)^{z-l} (1 \pm q_s)^l$ are the probabilities (6) evaluated at steady state values, and we introduced

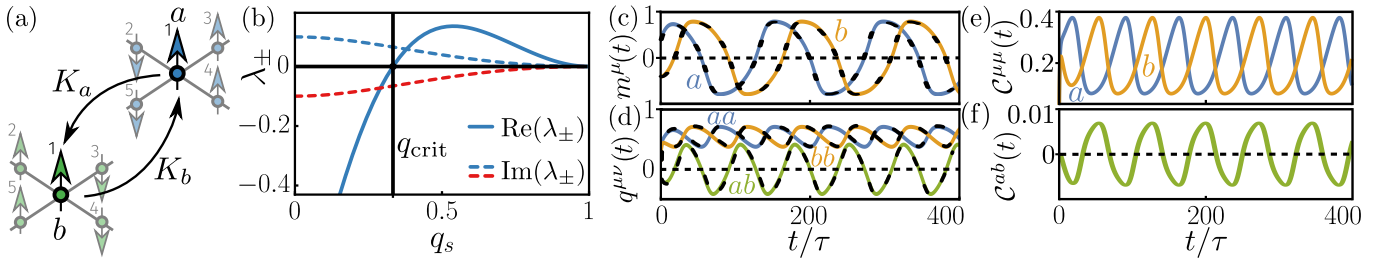


FIG. 1. (a) Schematic of a pair of Ising lattices a and b with coordination number $z = 4$ and cross-coupling (K_a, K_b) . For $K_a \neq K_b$ the cross-coupling is nonreciprocal. (b) Eigenvalues λ_{\pm} of the linear stability matrix (see Eq. (8)) as a function of the steady state short-range order q_s for $K_a = -K_b = 0.1$. When $q_s \geq q_{\text{crit}} \equiv 1/(z-1)$ (black vertical line) the real parts of λ_{\pm} are non-negative, resulting in coherent oscillations. (c-f) Temporal evolution of the magnetization (c; see Eq. (2)), (d) short-range order (see Eqs. (3)-(4)), and (e,f) short-range correlations $C^{\mu\nu}(t) \equiv q^{\mu\nu}(t) - m^{\mu}(t)m^{\nu}(t)$ for $K_a = -K_b = K = 0.1$ and $J_a = J_b = 0.4$. Black dashed lines in (c,d) are obtained with Monte-Carlo simulations on the Bethe lattice (see [56] for details). In all panels we consider $z = 4$.

the critical short-range order $q_{\text{crit}} \equiv 1/(z-1)$, which depends on the coordination number of the lattice. The solution of the linear stability equation can be written as $\delta\mathbf{m}(t) = \sum_{k=\pm} \mathcal{A}_k e^{\lambda_k t/\tau} \boldsymbol{\nu}_k$, where \mathcal{A}_{\pm} are set by the initial conditions, $\boldsymbol{\nu}_{\pm}$ are the eigenvectors of $\mathbf{M}(q_s; J, K)$ and $\lambda_{\pm}(q_s; J, K)$ the corresponding eigenvalues

$$\lambda_{\pm}(q_s; J, K) = M_{aa}(q_s; J, K) \pm iM_{ab}(q_s; J, K), \quad (8)$$

i being the imaginary unit. Since $M_{ab}(q_s; J, K \neq 0) \neq 0$ (see proof in [56]), the eigenvalues are complex for $K \neq 0$ (see dashed lines in Fig. 1b), resulting in oscillatory perturbations. The Hopf bifurcation [62], also called type-II_o instability [63], occurs when complex conjugate eigenvalues transit the imaginary axis in the complex plane. According to Eq. (8) this occurs when $M_{aa}(q_s; J, K) = 0$ implying $q_s(J, K) = q_{\text{crit}}$ as seen from Eq. (7). The Hopf bifurcation is thus set by the critical value q_{crit} for short-range order, and for $q_s > q_{\text{crit}}$ we have $\text{Re}(\lambda_{\pm}) > 0$ (solid line in Fig. 1b). In other words, when spins on the respective lattices are sufficiently aligned, a transition to an oscillatory state occurs (Fig. 1c,d). The critical value of the short-range order that determines the onset of coherent oscillations is our second main result that generalizes to other approximation schemes beyond the mean field approximation (see Appendix B).

Contrary to the idea that short-range order is slaved by long-range order [58], it rather seems that steady-state short-range order determines the bifurcation behavior of the long-range order. After sufficient short-range order is attained within the lattices, the frustration due to the nonreciprocal coupling gives rise to coherent oscillations: for $K > 0$ a spin σ_i^a wants to align with σ_i^b that in turn tends to misalign with σ_i^a . This dynamical frustration results in an oscillatory motion of the order parameters [16]. Notably, for the one-dimensional lattice ($z = 2$) we find $q_{\text{crit}} = 1$, which, in contrast to the mean-field prediction [49] (see also Appendix A), correctly implies the non-existence of a Hopf bifurcation.

Non-Linear analysis.—Going beyond linear stability, we perform a non-linear analysis of Eqs. (5) via numerical

continuation [64]. The resulting bifurcation diagrams are shown in Fig. 2(a,b) and the complete phase diagram in Fig. 2(d), which we now explain in detail.

We start with the non-interacting case with $K = 0$ (see Fig. 2a). For small values of J , there exists only one (trivial) stable steady state with $m_s^{\mu} = 0$, as explained in the previous section. Increasing J to $\ln(z/(z-2))/2$ we find a pitchfork bifurcation (red dot in Fig. 2a), which coincides with $q_s(J, 0) = q_{\text{crit}}$, and beyond which the trivial stable state becomes unstable. At the pitchfork bifurcation, 4 stable branches (blue lines in Fig. 2a) and 4 unstable branches (red dashed lines in Fig. 2a) emerge. The unstable branches are identified by a zero magnetization in either lattice, whereas the stable branches correspond to the spontaneously broken symmetry states with nonzero equilibrium magnetizations in both lattices.

Upon setting $K \neq 0$, the pitchfork bifurcation turns into a Hopf bifurcation (blue dot in Fig. 2b), whose J -value depends on K through the relation $q_s(J, K) = q_{\text{crit}}$ (blue line in Fig. 2d; see [56] for explicit results). Increasing J beyond the Hopf bifurcation, there is a regime with coherent oscillations (gray area in Fig. 2b,d). In Fig. 2d we identify the isolines of fixed period of the oscillations (black lines). Upon further increasing J at fixed K , we observe a non-linear transition from coherent oscillations to a non-zero stationary magnetization (light green region in Fig. 2d), which is set by a degenerate saddle-node-infinite-period (SNIPER) bifurcation (green dots in Fig. 2b). Approaching the SNIPER bifurcation from below, the magnetization in both lattices start to oscillate between four ghost states (see Fig. 2c), whereby the residence time within ghost states diverges as (see [56])

$$\mathcal{T} \propto (J_{\text{SNIP}}(K) - J)^{-1/2}, \quad (9)$$

where $J_{\text{SNIP}}(K)$ is the J -value of the SNIPER bifurcation at a given K (green line in Fig. 2d). At the SNIPER bifurcation, one unstable and stable branch merge, resulting in 4 unstable branches (red dashed lines in Fig. 2b) and 4 stable branches (blue lines in Fig. 2b). Note that these stable states with non-zero stationary magnetiza-

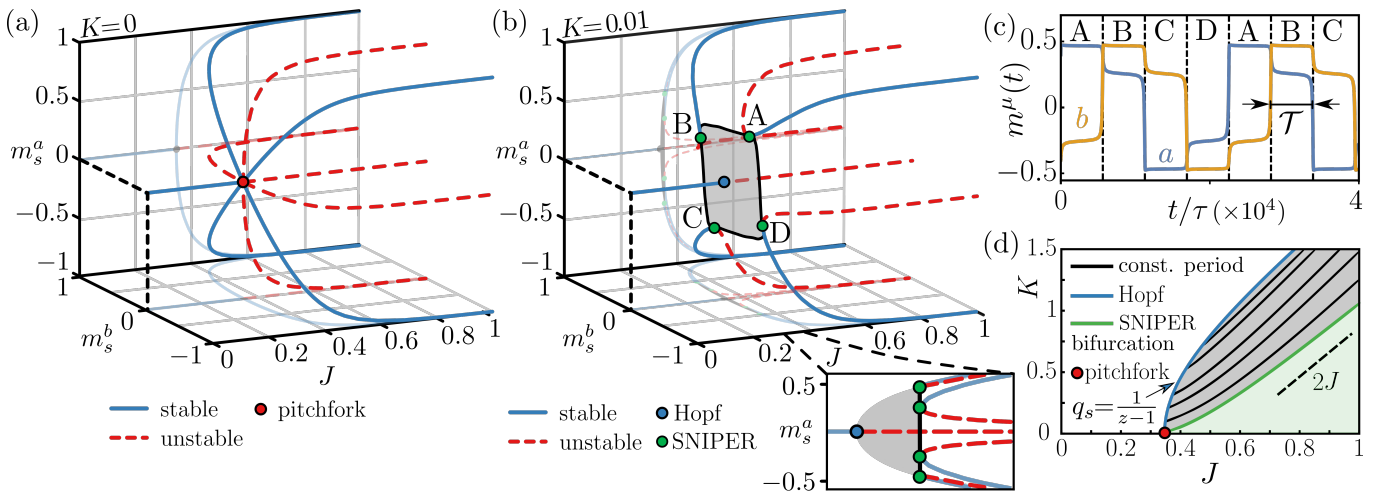


FIG. 2. (a,b) Bifurcation diagram of the magnetization (m_s^a, m_s^b) in the absence (a; $K = 0$) and presence (b; $K = 0.01$) of nonreciprocal coupling as a function of J . Inset of (b): Magnification of the bifurcation diagram around the Hopf bifurcation projected onto m_s^a . (c) Temporal evolution of the magnetization close to the degenerate saddle-node-infinite-period (SNIPER) bifurcation at $(J, K) = (0.35991, 0.01)$. The magnetization oscillates coherently between 4 ghost states $A \rightarrow B \rightarrow C \rightarrow D$ (for $K < 0$ the direction is reversed), which eventually terminate in the 4 respective stable branches at and beyond the SNIPER bifurcation. The life-time \mathcal{T} in these ghost states diverges upon approaching the SNIPER bifurcation at $J_{\text{SNIP}}(K)$ from the left as $\lim_{J \uparrow J_{\text{SNIP}}(K)} \mathcal{T} \propto (J_{\text{SNIP}}(K) - J)^{-1/2}$. (d) Phase diagram of m_s^a : the gray region depicts the regime of coherent oscillations, with the black lines indicating isolines with fixed oscillation period, and the blue line indicating the Hopf bifurcations where $q_s = q_{\text{crit}} \equiv 1/(z-1)$; in the light green region the magnetization is stationary and nonzero. In all panels we consider $z = 4$.

tion exist also in the square lattice system (see rigorous proof in [56]). This invalidates the hypothesis about the square lattice in Fig. 1d in [49].

The bifurcation diagram obtained with the mean-field approximation has similar qualitative features as in Fig. 2a,b (i.e. a Hopf and SNIPER bifurcation), however, the phase diagram displays a constant Hopf line at a fixed J , independent of K (see [49] and Fig. A1). In Fig. 2d we see that the Hopf line with the BG approximation is K -dependent, closely resembling the empirical phase diagram on the cubic lattice (see [49]). This highlights the non-trivial role of short-range order that is not included in the mean-field approximation.

Spatio-temporal dynamics.—The results in Fig. 1d-f reveal a high degree of local order in the coherent oscillatory regime. To systematically analyze the spatio-temporal patterns in states with coherent oscillations, we performed discrete-time Monte-Carlo simulations of the nonreciprocal Ising system with $2 \times N \approx 3 \times 10^3$ spins on the all-to-all ($z=N$), the $z=4$ Bethe, and the square ($z=4$) lattices with periodic boundary conditions. The respective systems are described in detailed in [56]. For a consistent notion of “spatial scale” on all lattices, we perform a graph-spectral analysis [65].

Let \mathbf{L} be the $N \times N$ symmetric Laplacian matrix of one of the above graphs with elements $L_{ii}=z$, and $L_{ij}=-1$ when spin i and j are connected and $L_{ij}=0$ otherwise. The Laplacian has N orthonormal eigenvectors $\mathbf{L}\psi_k=l_k\psi_k$, $k \in \{1, \dots, N\}$ with corresponding eigenvalues l_k ordered as $l_1 \leq l_2 \leq \dots \leq l_N$. The lowest eigenvalue, corresponding to $\psi_1=N^{-1/2}(1, \dots, 1)^T$, vanishes,

i.e., $l_1=0$ [66]. For the mean-field lattice, all remaining $N-1$ eigenvalues are degenerate, $l_2 = \dots = l_N = N$ [67], but not for the square and Bethe lattices (see [56]).

We express the microscopic state of the lattice μ at time-step $n \in \{0, \dots, n_{\text{max}}\}$ as a column vector $\sigma^\mu(n) = (\sigma_1^\mu(n), \dots, \sigma_N^\mu(n))^T$ and project it onto the respective eigenvectors, $\Psi_k^\mu(n) \equiv \psi_k^T \sigma^\mu(n)$. These spatial modes are shown as insets in Fig. 3a-c, where one can already see that for the Bethe and square lattice oscillations are pronounced on large scales (i.e. for small k) and severely suppressed on small scales (large k). In the mean-field system, the magnitude of (stochastic) oscillations is equal on all scales (all k) since the spectrum of \mathbf{L} is trivial.

To unravel the spatio-temporal structure, we compute the spectral density via the discrete Fourier transform,

$$\langle |\hat{\Psi}_k^\mu(\omega)| \rangle \equiv \left\langle \left| \sum_{n=0}^{n_{\text{max}}} |\Psi_k^\mu(n)| e^{-i2\pi\omega n/n_{\text{max}}} \right| \right\rangle, \quad (10)$$

where $\langle \cdot \rangle$ indicates averaging over independent trajectories and the absolute value takes into account that the sign of the projection is immaterial. The results are shown in Figs. 3a-c for coherent oscillations on the a lattice (those for the b lattice are equivalent), with resonances at even multiples of the respective natural frequency ω_0 . The spatio-temporal dynamics on the Bethe and square lattices is qualitatively the same, with small-scale and high-frequency modes severely suppressed. Thus, coherent oscillations are carried by large-scale low-frequency modes, which fully agrees with the large local correlations $\mathcal{C}^{\mu\mu}(t)$ within the respective lattices in Fig. 1e.

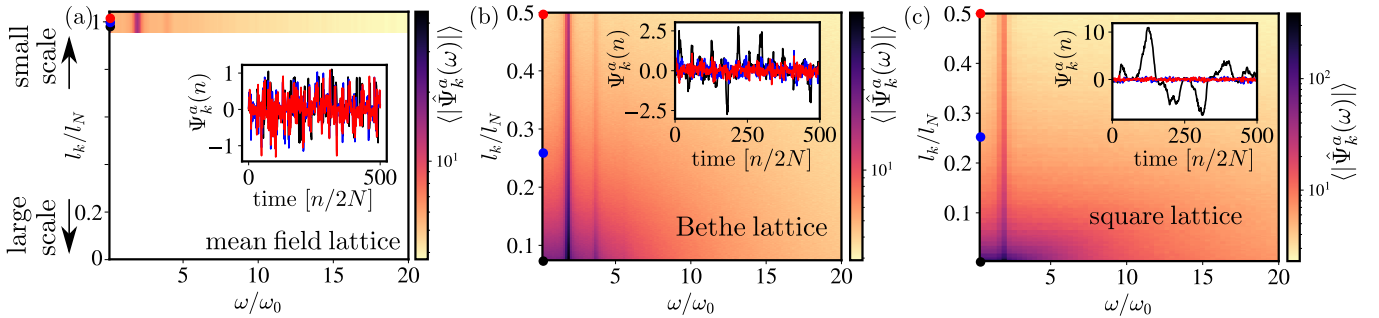


FIG. 3. (a-c) Spectral density $\langle |\hat{\Psi}_k^a(\omega)| \rangle$ of modes of coherent oscillations (Eq. (10)) on the (a) mean-field, (b) Bethe, and (c) square lattice. Note that the nonzero eigenvalues of the mean-field lattice are degenerate, which explains the white region in (a). The values for J are chosen in the respective oscillatory regimes (see [56] for details), and $K = 0.3$ for all three lattices. $\langle |\hat{\Psi}_k^a(\omega)| \rangle$ is averaged over 500 independent trajectories, and $\omega_0 = \text{argmax} \langle |\hat{\Psi}_k^a(\omega)| \rangle$ is the natural oscillation frequency. Resonances are visible at multiples of $2\omega_0$, since we ignore the sign of projections. Insets: Temporal development of the projected microscopic states onto the eigenvectors of the Laplacian matrix of respective lattices. Colors denote three selected eigenvalues (and thus spatial scales) indicated by the dots in the main plot.

Conclusion.—We explained the collective dynamics of the nonreciprocal Ising system on the level of both, local and global order. A critical threshold magnitude of nearest-neighbor correlations within the respective lattices was found to control the emergence of coherent oscillations of the global order parameter. Upon increasing interactions, ghost states emerge and the residence time in either of them eventually diverges, giving rise to a non-equilibrium steady state via a saddle-node-infinite-period bifurcation. Strikingly, during coherent oscillations of global order, a high degree of local order is preserved in nearest-neighbor-interacting systems. This implies non-trivial spatio-temporal correlations between spins, confirmed by a spectral-density maximum at large-scale low-frequency modes. In stark contrast, on the mean-field (all-to-all) lattice there is no distinction between different spatial modes, since each spin “feels” all spins, annihilating any notion of spatial structure. Thus, mean-field reasoning is insufficient; accounting for nearest-neighbor correlations is essential for a correct understanding of dynamics of nonreciprocal matter with short, or more generally finite, range of interactions.

Our work provides a comprehensive microscopic understanding of dynamic collective phenomena in nonreciprocal matter without conservation laws relevant, e.g. for enzyme clustering [68, 69]. What remains elusive are multiple (> 2) coupled lattices, spatially heterogeneous/extended systems [70], as well as the thermodynamic cost of dynamical states and bifurcations [54, 71–73]. These will be addressed in future works.

Acknowledgments.—Financial support from the German Research Foundation (DFG) through the Heisenberg Program Grants GO 2762/4-1 and GO 2762/5-1 (to AG) is gratefully acknowledged.

Appendix A: Mean-field approximation.—A less accurate technique to obtain approximate evolution equations is the mean-field (MF) approximation [49], where one

makes the rudimentary (uncontrolled) assumption

$$\langle \tanh(\Delta E_i^\mu/2) \rangle \approx \tanh \langle \Delta E_i^\mu/2 \rangle, \quad (\text{A1})$$

yielding the evolution equations

$$\begin{aligned} \tau \frac{dm^a(t)}{dt} + m^a(t) &= \tanh(zJ_a m^a(t) + K_a m^b(t)), \\ \tau \frac{dm^b(t)}{dt} + m^b(t) &= \tanh(zJ_b m^b(t) + K_b m^a(t)), \end{aligned} \quad (\text{A2})$$

which are exact on the fully connected mean-field lattice, where the local order is trivial (i.e. there is *no* sense of “local”), $q^{\mu\nu}(t) = m^\mu(t)m^\nu(t)$, and therefore $\mathcal{C}^{\mu\nu}(t) = 0$. A linear stability analysis around the trivial steady-state $m_s^\mu = 0$ for $J_a = J_b = J$ and $K_a = -K_b = K$ leads to the linear stability equation $\tau d\delta\mathbf{m}(t)/dt = \mathbf{M}^{\text{MF}}(J, K)\delta\mathbf{m}(t)$ with elements

$$M_{aa}^{\text{MF}} = M_{bb}^{\text{MF}} = zJ - 1, \quad (\text{A3})$$

$$M_{ab}^{\text{MF}} = -M_{ba}^{\text{MF}} = K. \quad (\text{A4})$$

The eigenvalues of \mathbf{M}^{MF} are given by

$$\lambda_{\pm}^{\text{MF}}(J, K) = (zJ - 1) \pm iK. \quad (\text{A5})$$

Hence, the Hopf bifurcation occurs at $J = 1/z$ and $K \neq 0$, such that $\text{Re}(\lambda_{\pm}^{\text{MF}}) = 0$ and $\text{Im}(\lambda_{\pm}^{\text{MF}}) \neq 0$. This corresponds to a straight vertical line in the (J, K) -plane, as shown in Fig. A1a, which is unphysical for short range interactions. Notably, in the MF approximation we do *not* observe a critical value for short-range order, which is present in the more accurate BG approximation.

Appendix B: Monomer approximation.—Another approximation technique we developed in this work is what we call the “monomer approximation”. It is more accurate than the MF yet less accurate than the BG approximation.

The conceptual difference between the MF on the one hand, and the monomer and BG approximations

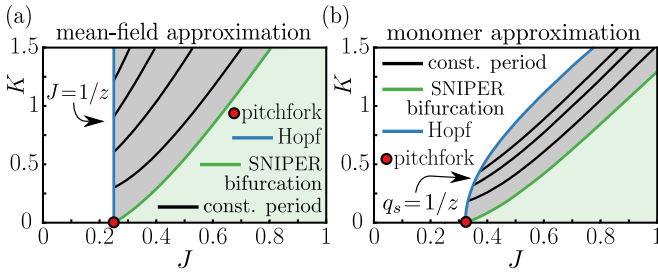


FIG. A1. Phase diagram for global order m_s^μ obtained with the mean-field (MF) approximation (a) and the monomer approximation (b) for the perfect nonreciprocal setting with $J_a = J_b = J$ and $K_a = -K_b = K$. In the MF approximation the Hopf bifurcation (blue line) is set by $J = 1/z$. In the monomer approximation, the Hopf bifurcations (blue line) is set by a critical short-range order $q_s = 1/z$, which is more similar to the Bethe-Guggenheim approximation where $q_s = 1/(z-1)$ (see Fig. 2d).

TABLE I. Overview of approximation techniques and their dynamical equations

approx. technique	$m^\mu(t)$	$q^{\mu\nu}(t)$	Hopf
MF	(A2)	$= m^\mu(t)m^\nu(t)$	$J=1/z$
monomer	(5)+(B2)	(5)+(B2); slaved by $m^\mu(t)$	$q_s=1/z$
BG	(5)+(6)	(5)+(6); not slaved	$q_s=1/(z-1)$

on the other hand lies in the treatment of the average $\langle \tanh(\Delta E_i^\mu/2) \rangle$. Whereas the MF approximation simply moves the average to the argument as shown in Eq. (A1), the monomer and BG approximations use the fact that the value of $\Delta E_i^\mu/2$ lies in an enumerable set given by $U_{l,n}^\mu \equiv [2l-z]J_\mu + [2n-1]K_\mu$ with $l \in \{0, \dots, z\}$ and $n \in \{0, 1\}$. This allows for an explicit summation

$$\langle \tanh(\Delta E_i^\mu/2) \rangle = \sum_{l=0}^z \sum_{n=0}^1 \mathcal{P}_{l,n}^\mu(t) \tanh(U_{l,n}^\mu), \quad (\text{B1})$$

where only the probability $\mathcal{P}_{l,n}^\mu(t)$ has to be approximated.

Similarly to the BG approximation, the resulting evolution equations in the monomer approximation are governed by Eqs. (5), but the time-dependent probabilities are different and read (the derivation is given in [56])

$$\mathcal{P}_{l,n}^a(t) = \frac{2\mathcal{C}_l^z (1+m^a(t))^l (1+m^b(t))^n}{(1-m^a(t))^{l-z} (1-m^b(t))^{n-1}}, \quad (\text{B2})$$

and $\mathcal{P}_{l,n}^b(t)$ is obtained by replacing $m^a(t)$ with $m^b(t)$ in Eq. (B2). Since $\mathcal{P}_{l,n}^a(t)$ is independent of the short-range order $q^{\mu\nu}(t)$, this implies that $q^{\mu\nu}(t)$ is slaved by $m^\mu(t)$, however, $q^{\mu\nu}(t) \neq m^\mu(t)m^\nu(t)$. Performing a linear stability analysis around the trivial steady-state $m_s^\mu = 0$ for $J_a = J_b = J$ and $K_a = -K_b = K$, we obtain the linear stability equation $\tau d\delta\mathbf{m}(t)/dt = \hat{\mathbf{M}}(J, K)\delta\mathbf{m}(t)$ where the elements of $\hat{\mathbf{M}}(J, K)$ are given by

$$\hat{M}_{aa} = \hat{M}_{bb} = 2 \sum_{l=0}^z \sum_{n=0}^1 (2l-z)\mathcal{C}_l^z \tanh(U_{l,n}^a) - 1, \quad (\text{B3})$$

$$\hat{M}_{ab} = -\hat{M}_{ba} = 2 \sum_{l=0}^z \sum_{n=0}^1 (2n-1)\mathcal{C}_l^z \tanh(U_{l,n}^a). \quad (\text{B4})$$

Interestingly, Eq. (B3) can be expressed in terms of the steady-state value of the short-range order in the monomer approximation, i.e., $\hat{M}_{aa}(J, K) = zq_s(J, K) - 1$. Therefore, the eigenvalues of $\hat{\mathbf{M}}(J, K)$ are neatly given by

$$\hat{\lambda}_\pm(J, K) = (zq_s(J, K) - 1) \pm i\hat{M}_{ab}(J, K). \quad (\text{B5})$$

Herefrom it follows that the Hopf bifurcation occurs at $q_s = 1/z$ and $K \neq 0$, such that $\text{Re}(\hat{\lambda}_\pm) = 0$ and $\text{Im}(\hat{\lambda}_\pm) \neq 0$. Hence, as within the BG approximation, we also find the existence of a critical short-range order in the monomer approximation. Contrary to the MF approximation, the Hopf line is *not* a straight vertical line in the (J, K) -plane, as shown in Fig. A1b.

Appendix C: Local and global order in various approximations.—To provide a concise overview of the various approximation techniques, we summarize in Table I the respective evolution and conditions for the Hopf bifurcation.

-
- [1] M. Fruchart, R. Hanai, P. B. Littlewood, and V. Vitelli, *Nature* **592**, 363 (2021).
 - [2] F. Brauns and M. C. Marchetti, *Phys. Rev. X* **14**, 021014 (2024).
 - [3] Z.-F. Huang, M. te Vrugt, R. Wittkowski, and H. Löwen, *Active pattern formation emergent from single-species nonreciprocity* (2024), arXiv:2404.10093 [cond-mat.soft].
 - [4] K. Ishimoto, C. Moreau, and K. Yasuda, *PRX Life* **1**, 023002 (2023).
 - [5] A. Najafi and R. Golestanian, *Phys. Rev. E* **69**, 062901 (2004).
 - [6] P. R. Buenzli and R. Soto, *Phys. Rev. E* **78**, 020102 (2008).
 - [7] C. H. Meredith, P. G. Moerman, J. Groenewold, Y.-J. Chiu, W. K. Kegel, A. van Blaaderen, and L. D. Zarzar, *Nat. Chem.* **12**, 1136 (2020).
 - [8] A. M. Mambuca, C. Cammarota, and I. Neri, *Phys. Rev. E* **105**, 014305 (2022).
 - [9] L. Guislain and E. Bertin, *Collective oscillations in a three-dimensional spin model with non-reciprocal interactions* (2024), arXiv:2405.13925 [cond-mat.stat-mech].
 - [10] S. A. M. Loos, S. H. L. Klapp, and T. Martynek, *Phys. Rev. Lett.* **130**, 198301 (2023).
 - [11] L. Guislain and E. Bertin, *Phys. Rev. E* **109**, 034131 (2024).

- [12] S. Osat and R. Golestanian, *Nat. Nanotechnol.* **18**, 79 (2023).
- [13] S. Osat, J. Metson, M. Kardar, and R. Golestanian, Escaping kinetic traps using non-reciprocal interactions (2023), [arXiv:2309.00562](https://arxiv.org/abs/2309.00562) [cond-mat.stat-mech].
- [14] D. S. Seara, A. Piya, and A. P. Tabatabai, *J. Stat. Mech.: Theory Exp.* **2023** (4), 043209.
- [15] H. Rieger, M. Schreckenberg, and J. Zittartz, *Z. Phys.* **74**, 527 (1989).
- [16] R. Hanai, *Phys. Rev. X* **14**, 011029 (2024).
- [17] L. Guislain and E. Bertin, Hidden collective oscillations in a disordered mean-field spin model with non-reciprocal interactions (2024), [arXiv:2406.03874](https://arxiv.org/abs/2406.03874) [cond-mat.dis-nn].
- [18] C. Scheibner, A. Souslov, D. Banerjee, P. Surówka, W. T. Irvine, and V. Vitelli, *Nat. Phys.* **16**, 475 (2020).
- [19] B. Bhattacharjee, M. Hayakawa, and T. Shibata, *Soft Matter* **20**, 2739 (2024).
- [20] Y. Yifat, D. Coursault, C. W. Peterson, J. Parker, Y. Bao, S. K. Gray, S. A. Rice, and N. F. Scherer, *Light Sci. Appl.* **7**, 105 (2018).
- [21] J. Parker, C. W. Peterson, Y. Yifat, S. A. Rice, Z. Yan, S. K. Gray, and N. F. Scherer, *Optica* **7**, 1341 (2020).
- [22] A. V. Ivlev, J. Bartnick, M. Heinen, C.-R. Du, V. Novenko, and H. Löwen, *Phys. Rev. X* **5**, 011035 (2015).
- [23] A. Ivlev, G. Morfill, H. Löwen, and C. P. Royall, *Complex plasmas and colloidal dispersions: particle-resolved studies of classical liquids and solids*, Vol. 5 (World Scientific Publishing Company, 2012).
- [24] M. Bonitz, C. Henning, and D. Block, *Rep. Prog. Phys.* **73**, 066501 (2010).
- [25] Z. You, A. Baskaran, and M. C. Marchetti, *Proc. Natl. Acad. Sci. U.S.A.* **117**, 19767 (2020).
- [26] J. Agudo-Canalejo and R. Golestanian, *Phys. Rev. Lett.* **123**, 018101 (2019).
- [27] R. Soto and R. Golestanian, *Phys. Rev. Lett.* **112**, 068301 (2014).
- [28] S. Saha, S. Ramaswamy, and R. Golestanian, *New J. Phys.* **21**, 063006 (2019).
- [29] N. S. Mandal, A. Sen, and R. D. Astumian, *Chem* **10**, 1147 (2024).
- [30] V. Ouazan-Reboul, J. Agudo-Canalejo, and R. Golestanian, *Nat. Commun.* **14**, 4496 (2023).
- [31] A. Dinelli, J. O’Byrne, A. Curatolo, Y. Zhao, P. Sollich, and J. Tailleur, *Nat. Commun.* **14**, 7035 (2023).
- [32] T. Nadolny, C. Bruder, and M. Brunelli, Nonreciprocal synchronization of active quantum spins (2024), [arXiv:2406.03357](https://arxiv.org/abs/2406.03357) [quant-ph].
- [33] A. Metelmann and A. A. Clerk, *Phys. Rev. X* **5**, 021025 (2015).
- [34] B. Ahmadi, P. Mazurek, P. Horodecki, and S. Barzanjeh, *Phys. Rev. Lett.* **132**, 210402 (2024).
- [35] J. Garnier-Brun, M. Benzaquen, and J.-P. Bouchaud, *Phys. Rev. X* **14**, 021039 (2024).
- [36] H. Hong and S. H. Strogatz, *Phys. Rev. Lett.* **106**, 054102 (2011).
- [37] H. Rieger, M. Schreckenberg, and J. Zittartz, *J. Phys. A* **21**, L263 (1988).
- [38] T. Takahashi, *Med. hypotheses* **68**, 184 (2007).
- [39] M. Brandenbourger, X. Locsin, E. Lerner, and C. Coullais, *Nat. Commun.* **10**, 4608 (2019).
- [40] M. te Vrugt, M. P. Holl, A. Koch, R. Wittkowski, and U. Thiele, *Model. Simul. Mater. Sci. Eng.* **30**, 084001 (2022).
- [41] T. Frohoff-Hülsmann, J. Wrembel, and U. Thiele, *Phys. Rev. E* **103**, 042602 (2021).
- [42] S. Saha, J. Agudo-Canalejo, and R. Golestanian, *Phys. Rev. X* **10**, 041009 (2020).
- [43] K. John and M. Bär, *Phys. Rev. Lett.* **95**, 198101 (2005).
- [44] T. Frohoff-Hülsmann and U. Thiele, *IMA J. Appl. Math.* **86**, 924 (2021).
- [45] T. Frohoff-Hülsmann, M. P. Holl, E. Knobloch, S. V. Gurevich, and U. Thiele, *Phys. Rev. E* **107**, 064210 (2023).
- [46] R. Mandal, S. S. Jaramillo, and P. Sollich, *Phys. Rev. E* **109**, L062602 (2024).
- [47] T. Frohoff-Hülsmann, U. Thiele, and L. M. Pismen, *Phil. Trans. R. Soc. A* **381**, 20220087 (2023).
- [48] P. C. Hohenberg and B. I. Halperin, *Rev. Mod. Phys.* **49**, 435 (1977).
- [49] Y. Avni, M. Fruchart, D. Martin, D. Seara, and V. Vitelli, The non-reciprocal Ising model (2023), [arXiv:2311.05471](https://arxiv.org/abs/2311.05471) [cond-mat.stat-mech].
- [50] M. Liu, Z. Hou, H. Kitahata, L. He, and S. Komura, *J. Phys. Soc. Jpn.* **92**, 093001 (2023).
- [51] D. Schüler, S. Alonso, A. Torcini, and M. Bär, *Chaos* **24**, 043142 (2014).
- [52] D. Zwicker, A. A. Hyman, and F. Jülicher, *Phys. Rev. E* **92**, 012317 (2015).
- [53] C. A. Weber, D. Zwicker, F. Jülicher, and C. F. Lee, *Rep. Prog. Phys.* **82**, 064601 (2019).
- [54] T. Suchanek, K. Kroy, and S. A. M. Loos, *Phys. Rev. Lett.* **131**, 258302 (2023).
- [55] The local interaction is not equal to the total energy of the system, since the interaction energy for the two lattices a and b is different.
- [56] See Supplementary Material at [...].
- [57] R. J. Glauber, *J. Math. Phys.* **4**, 294 (1963).
- [58] Y. Saito and R. Kubo, *J. Stat. Phys.* **15**, 233 (1976).
- [59] K. Blom, *Pair-Correlation Effects in Many-Body Systems: Towards a Complete Theoretical Description of Pair-Correlations in the Static and Kinetic Description of Many-Body Systems* (Springer Nature, Cham, Switzerland, 2023).
- [60] D. A. Johnston and P. Plechác, *J. Phys. A: Math. Gen.* **31**, 475 (1998).
- [61] D. Dhar, P. Shukla, and J. P. Sethna, *J. Phys. A: Math. Gen.* **30**, 5259 (1997).
- [62] S. H. Strogatz, *Nonlinear dynamics and chaos: with applications to physics, biology, chemistry, and engineering* (CRC press, Boca Raton, USA, 2018).
- [63] M. C. Cross and P. C. Hohenberg, *Rev. Mod. Phys.* **65**, 851 (1993).
- [64] A. Dhooge, W. Govaerts, and Y. A. Kuznetsov, *ACM Trans. Math. Softw.* **29**, 141–164 (2003).
- [65] J. van der Kolk, G. García-Pérez, N. E. Kouvaris, M. A. Serrano, and M. Boguñá, *Phys. Rev. X* **13**, 021038 (2023).
- [66] W. N. Anderson Jr and T. D. Morley, *Linear and multilinear algebra* **18**, 141 (1985).
- [67] R. Cohen and S. Havlin, *Complex networks: structure, robustness and function* (Cambridge university press, 2010).
- [68] A. Buchner, F. Tostevin, and U. Gerland, *Phys. Rev. Lett.* **110**, 208104 (2013).
- [69] F. Hinzpeter, F. Tostevin, A. Buchner, and U. Gerland, *Nat. Phys.* **18**, 203–211 (2021).
- [70] K. Blom, N. Ziethen, D. Zwicker, and A. Godec, *Phys. Rev. Res.* **5**, 013135 (2023).
- [71] C. Nardini, E. Fodor, E. Tjhung, F. van Wijland, J. Tailleur, and M. E. Cates, *Phys. Rev. X* **7**, 021007 (2017).

- (2017).
- [72] K. Blom, K. Song, E. Vouga, A. Godec, and D. E. Makarov, *Proc. Natl. Acad. Sci. U.S.A.* **121**, e2318333121 (2024).
- [73] Z. Zhang and R. Garcia-Millan, *Phys. Rev. Res.* **5**, L022033 (2023).

Supplementary Material for: Interplay between local and global order controls bifurcations in nonreciprocal systems without a conservation law

Kristian Blom¹, Uwe Thiele^{2,3,4}, and Aljaž Godec¹

¹*Mathematical bioPhysics Group, Max Planck Institute for Multidisciplinary Sciences, 37077 Göttingen, Germany*

²*Institute of Theoretical Physics, University of Münster, Münster 48149, Germany*

³*Center for Nonlinear Science (CeNoS), University of Münster, Münster 48149, Germany*

⁴*Center for Multiscale Theory and Computation (CMTC), University of Münster, Münster 48149, Germany*

In this Supplemental Material, we provide derivations and further details about the results shown in the Letter. Furthermore, in Sec. S6 we prove that static long-range order in the square-lattice Ising model persists under small perturbations in the nonreciprocal coupling K , which invalidates a recent hypothesis [1].

CONTENTS

S1. Setup: Dual lattice topology and interactions	2
S2. Glauber dynamics	2
S3. Differential equations for the long- and short-range order	2
S3.1. The “monomer” approximation	4
S3.1.1. Difference with respect to mean-field approximation	4
S3.2. The Bethe-Guggenheim “pair” approximation	5
S4. Linear stability analysis	6
S4.1. The “monomer” approximation	6
S4.1.1. Perfectly nonreciprocal setting	7
S4.2. The Bethe-Guggenheim “pair” approximation	7
S4.2.1. Steady-state short-range order	7
S4.2.2. Linear stability of long-range order	8
S4.2.3. Linear stability of short-range order	9
S5. Divergence of the residence time upon approaching the SNIPER bifurcation	10
S6. Proof of existence of static long-range order on the square lattice	11
S6.1. Recap of the long-range order	11
S6.2. Steady-state for $K = 0$	12
S6.3. Perturbation expansion in K	12
S6.4. Bound on perturbations of long-range order	13
S6.5. Connecting the dots and final remark	14
S7. Kinetic Monte-Carlo simulations	14
S7.1. Simulation setup	15
S7.2. Eigenvalues of Laplacian matrix	15
References	16

S1. SETUP: DUAL LATTICE TOPOLOGY AND INTERACTIONS

Consider a pair of lattices, denoted by $\mu = a, b$, each having a coordination number z and periodic boundary conditions. On each lattice there are N spins that can be in two states $\sigma_i^\mu = \pm 1$, with $i \in \{1, \dots, N\}$ enumerating the spin's location. Each spin interacts with its z nearest-neighbors on the same lattice and one spin at the equivalent position on the opposing lattice. The *local* interaction energy of spin i on lattice μ can be written as (see also [1])

$$E_i^\mu = -J_\mu \sigma_i^\mu \sum_{\langle i|j \rangle} \sigma_j^\mu - K_\mu \sigma_i^a \sigma_i^b, \quad (\text{S1})$$

where $\langle i|j \rangle$ denotes a sum over nearest-neighbors j of spin i . Throughout, we will express energies in units of $k_B T$. The parameters J_μ and K_μ denote the coupling within one and between the two lattices, respectively. When $K_a \neq K_b$, equivalent spins in the opposing lattices interact nonreciprocally.

S2. GLAUBER DYNAMICS

We now specify the dynamics. We consider single spin-flip dynamics according to Glauber [2]. Let $P(\boldsymbol{\sigma}; t)$ be the probability at time t to be in state $\boldsymbol{\sigma} = \{\sigma_1^a, \sigma_1^b, \dots, \sigma_N^a, \sigma_N^b\}$. This state can be reached by a single spin flip from the $2N$ distinct states $\boldsymbol{\sigma}'_{\mu,i} = \{\sigma_1^a, \sigma_1^b, \dots, -\sigma_i^\mu, \dots, \sigma_N^a, \sigma_N^b\}$, which enters the master equation as follows

$$\frac{dP(\boldsymbol{\sigma}; t)}{dt} = \sum_{\mu=a,b} \sum_{i=1}^N [w_i^\mu(-\sigma_i^\mu) P(\boldsymbol{\sigma}'_{\mu,i}; t) - w_i^\mu(\sigma_i^\mu) P(\boldsymbol{\sigma}; t)]. \quad (\text{S2})$$

The respective transition rates $w_i^\mu(\sigma_i^\mu)$ to flip a single spin $\sigma_i^\mu \rightarrow -\sigma_i^\mu$ can be specified uniquely by limiting the interactions to nearest neighbors, imposing isotropy in position space, and requiring that for $K_a = K_b$ the transition rates obey detailed-balance. These physical restrictions then lead to the general result

$$w_i^\mu(\sigma_i^\mu) = (1/2\tau) [1 - \tanh(\Delta E_i^\mu/2)], \quad (\text{S3})$$

where ΔE_i^μ is the change in energy on the $\mu = a \vee b$ lattice after flipping spin $\sigma_i^\mu \rightarrow -\sigma_i^\mu$, and $\tau \equiv 2N$ is an intrinsic timescale to attempt a spin-flip. According to Eq. (S1), the change in energy after such a spin-flip is given by

$$\Delta E_i^\mu = -2E_i^\mu. \quad (\text{S4})$$

From the master equation (S2), we can directly derive equations for the first two moments of single-spin values (see also Eqs. (28) and (29) in [2])

$$\tau \frac{d\langle \sigma_i^\mu(t) \rangle}{dt} + \langle \sigma_i^\mu(t) \rangle = \langle \sigma_i^\mu(t) \tanh(\Delta E_i^\mu/2) \rangle, \quad (\text{S5})$$

$$\tau \frac{d\langle \sigma_i^\mu(t) \sigma_j^\nu(t) \rangle}{dt} + 2\langle \sigma_i^\mu(t) \sigma_j^\nu(t) \rangle = \langle \sigma_i^\mu(t) \sigma_j^\nu(t) [\tanh(\Delta E_i^\mu/2) + \tanh(\Delta E_j^\nu/2)] \rangle, \quad (\text{S6})$$

where $\langle f(t) \rangle \equiv \sum_{\boldsymbol{\sigma}} P(\boldsymbol{\sigma}; t) f(\boldsymbol{\sigma})$. Eqs. (S5)-(S6) are exact (but *not* yet closed) equations for the first two moments evolving under Glauber dynamics, and will serve as our starting point to derive equations for the long- and short-range order parameters.

S3. DIFFERENTIAL EQUATIONS FOR THE LONG- AND SHORT-RANGE ORDER

Recall from the Letter that the long- and short-range order are defined as

$$m^\mu(t) \equiv \frac{1}{N} \sum_{i=1}^N \langle \sigma_i^\mu(t) \rangle, \quad (\text{S7})$$

$$q^{\mu\mu}(t) \equiv \frac{2}{zN} \sum_{i=1}^N \sum_{\langle i|j \rangle} \langle \sigma_i^\mu(t) \sigma_j^\mu(t) \rangle, \quad (\text{S8})$$

$$q^{ab}(t) \equiv \frac{1}{N} \sum_{i=1}^N \langle \sigma_i^a(t) \sigma_i^b(t) \rangle. \quad (\text{S9})$$

Here, we rewrite Eqs. (S5)-(S6) in terms of differential equations for (S7)-(S9), which we do in two steps:

1. First, we sum Eqs. (S5)-(S6) over all spins and spin pairs. Upon doing this, the l.h.s. of Eqs. (S5)-(S6) directly transforms into

$$\frac{1}{N} \sum_{i=1}^N \left(\tau \frac{d\langle \sigma_i^\mu(t) \rangle}{dt} + \langle \sigma_i^\mu(t) \rangle \right) = \tau \frac{dm^\mu(t)}{dt} + m^\mu(t), \quad (\text{S10})$$

$$\frac{2}{zN} \sum_{i=1}^N \sum_{\langle i|j \rangle} \left(\tau \frac{d\langle \sigma_i^\mu(t) \sigma_j^\mu(t) \rangle}{dt} + 2\langle \sigma_i^\mu(t) \sigma_j^\mu(t) \rangle \right) = \tau \frac{dq^{\mu\mu}(t)}{dt} + 2q^{\mu\mu}(t), \quad (\text{S11})$$

$$\frac{1}{N} \sum_{i=1}^N \left(\tau \frac{d\langle \sigma_i^a(t) \sigma_i^b(t) \rangle}{dt} + 2\langle \sigma_i^a(t) \sigma_i^b(t) \rangle \right) = \tau \frac{dq^{ab}(t)}{dt} + 2q^{ab}(t). \quad (\text{S12})$$

2. Next, we need to evaluate the r.h.s. of Eqs. (S5)-(S6) after summation over all spins and spin pairs. To do this, we make use of the fact that ΔE_i^μ can take on a discrete (enumerable) set of values. Let us consider a spin with $l \in \{0, 1, \dots, z\}$ neighboring up spins on the same lattice, and $n \in \{0, 1\}$ neighboring up spins on the opposing lattice. We want to compute the change in energy upon flipping this spin. Based on Eq. (S4) we can parameterize the change in energy after flipping a spin with such an environment as follows,

$$\Delta E_i^\mu = 2\sigma_i^\mu U_{l,n}^\mu, \quad (\text{S13})$$

where

$$U_{l,n}^\mu = [2l - z]J_\mu + [2n - 1]K_\mu. \quad (\text{S14})$$

This gives a direct parameterization of the energy change in terms of the number of neighboring up spins on the same (l) and opposing (n) lattice. Using this parameterization, we can evaluate the r.h.s. of Eqs. (S5)-(S6) using the following identities

$$\frac{1}{N} \sum_{i=1}^N \langle \sigma_i^\mu \tanh(\Delta E_i^\mu/2) \rangle = \frac{1}{N} \sum_{i=1}^N \langle \tanh(U_{l,n}^\mu) \rangle = \sum_{l=0}^z \sum_{n=0}^1 \mathcal{P}_{l,n}^\mu(t) \tanh(U_{l,n}^\mu), \quad (\text{S15})$$

$$\frac{2}{zN} \sum_{i=1}^N \sum_{\langle i|j \rangle} \langle \sigma_i^\mu \sigma_j^\mu \tanh(\Delta E_i^\mu/2) \rangle = \frac{2}{zN} \sum_{i=1}^N \sum_{\langle i|j \rangle} \langle \sigma_j^\mu \tanh(U_{l,n}^\mu) \rangle = \frac{2}{z} \sum_{l=0}^z \sum_{n=0}^1 (2l - z) \mathcal{P}_{l,n}^\mu(t) \tanh(U_{l,n}^\mu), \quad (\text{S16})$$

$$\frac{1}{N} \sum_{i=1}^N \langle \sigma_i^a \sigma_i^b \tanh(\Delta E_i^a/2) \rangle = \frac{1}{N} \sum_{i=1}^N \langle \sigma_i^b \tanh(U_{l,n}^a) \rangle = \sum_{l=0}^z \sum_{n=0}^1 (2n - 1) \mathcal{P}_{l,n}^\mu(t) \tanh(U_{l,n}^a). \quad (\text{S17})$$

For the first equality in Eqs. (S15)-(S17) we used that $\tanh(\Delta E_i^\mu/2) = \tanh(\sigma_i^\mu U_{l,n}^\mu) = \sigma_i^\mu \tanh(U_{l,n}^\mu)$, together with $(\sigma_i^\mu)^2 = 1$. For the second equality, we used that terms like $\langle \tanh(U_{l,n}^\mu) \rangle$ represent a weighted sum over all possible combinations of the possible values that $\tanh(U_{l,n}^\mu)$ can attain. The weights are given by the time-dependent probability $\mathcal{P}_{l,n}^\mu(t)$ to find an up or down spin with a specific local environment. By definition, this probability is normalized as,

$$\sum_{l=0}^z \sum_{n=0}^1 \mathcal{P}_{l,n}^\mu(t) = 1. \quad (\text{S18})$$

Combining Eqs. (S10)-(S12) and (S15)-(S17) we obtain

$$\tau \frac{dm^\mu(t)}{dt} + m^\mu(t) = \sum_{l=0}^z \sum_{n=0}^1 \mathcal{P}_{l,n}^\mu(t) \tanh(U_{l,n}^\mu), \quad (\text{S19})$$

$$\tau \frac{dq^{\mu\mu}(t)}{dt} + 2q^{\mu\mu}(t) = \frac{2}{z} \sum_{l=0}^z \sum_{n=0}^1 (2l - z) \mathcal{P}_{l,n}^\mu(t) \tanh(U_{l,n}^\mu), \quad (\text{S20})$$

$$\tau \frac{dq^{ab}(t)}{dt} + 2q^{ab}(t) = \sum_{\mu=a,b} \sum_{l=0}^z \sum_{n=0}^1 (2n - 1) \mathcal{P}_{l,n}^\mu(t) \tanh(U_{l,n}^\mu), \quad (\text{S21})$$

corresponding to Eq. (5) in the Letter. Our next aim is to obtain closed-form expressions for $\mathcal{P}_{l,n}^\mu(t)$, for which we consider two approximation techniques: the ‘‘monomer’’ approximation, and the Bethe-Guggenheim (BG) approximation.

S3.1. The “monomer” approximation

We start with the lowest-order approximation, where we neglect nearest-neighbor correlations in the probability $\mathcal{P}_{l,n}^\mu$. Note, however, that already this level of approximation goes beyond the mean-field approach in [1]. Suppose we want to know the probability of finding an up or down spin on the a lattice which has l nearest up neighbors on the a lattice and n nearest up neighbors on the b lattice. On the monomer level we assume perfect mixing between the up and down spins, resulting in

$$\mathcal{P}_{l,n}^a = \underbrace{\left[\binom{N_+^a}{l} \binom{N_-^a}{z-l} / \binom{N_+^a + N_-^a}{z} \right]}_{\substack{\text{probability for} \\ l \text{ neighboring up} \\ \text{spins on the } a \text{ lattice}}} \times \underbrace{\left[\binom{N_+^b}{n} \binom{N_-^b}{1-n} / \binom{N_+^b + N_-^b}{1} \right]}_{\substack{\text{probability for} \\ n \text{ neighboring up} \\ \text{spins on the } b \text{ lattice}}}, \quad (\text{S22})$$

where N_+^μ is the total number of up spins on the μ lattice, and similarly N_-^μ the total number of down spins. The same reasoning applies to the probability $\mathcal{P}_{l,n}^b$. Note that N_\pm^μ is generally time-dependent, but for simplicity we omit the subscript t . To relate N_\pm^μ to the long-range order we use the following relations (omitting the time dependence subscript t)

$$m^\mu = (N_+^\mu - N_-^\mu)/N, \quad (\text{S23})$$

$$N = N_+^\mu + N_-^\mu, \quad (\text{S24})$$

from which follows that

$$N_\pm^\mu = N(1 \pm m^\mu)/2. \quad (\text{S25})$$

Inserting this back into Eq. (S22) and taking the thermodynamic limit, i.e. the scaling limit $N \rightarrow \infty$ while keeping $\mathbf{m}(t) \equiv (m^a(t), m^b(t))$ fixed, we can make use of the following result for the binomial coefficients

$$\lim_{N \rightarrow \infty}^{m^\mu = \text{const.}} \binom{N(1 \pm m^\mu)/2}{l} \simeq \frac{(N(1 \pm m^\mu)/2)^l}{l!}, \quad \text{for } l \in \mathbb{N} \quad (\text{S26})$$

where \simeq stands for asymptotic equality. Inserting Eq. (S26) into Eq. (S22), and restoring the explicit time-dependence, we finally obtain (note that the N dependence cancels out)

$$\mathcal{P}_{l,n}^a(t) \simeq \frac{2\mathcal{C}_l^z (1 + m^a(t))^l (1 + m^b(t))^n}{(1 - m^a(t))^{l-z} (1 - m^b(t))^{n-1}}, \quad (\text{S27})$$

$$\mathcal{P}_{l,n}^b(t) \simeq \frac{2\mathcal{C}_l^z (1 + m^b(t))^l (1 + m^a(t))^n}{(1 - m^b(t))^{l-z} (1 - m^a(t))^{n-1}}, \quad (\text{S28})$$

where

$$\mathcal{C}_l^z \equiv \frac{1}{2^{z+2}} \binom{z}{l}. \quad (\text{S29})$$

Hence, in the monomer approximation, we find that the probability $\mathcal{P}_{l,n}^\mu(t)$ only explicitly depends on the long-range order $\mathbf{m}(t)$, and *not* on the short-range order $\mathbf{q}(t) \equiv (q^{aa}(t), q^{bb}(t), q^{ab}(t))$. Upon inserting Eq. (S27) into Eqs. (S19)-(S21) we obtain a closed set of five non-linear differential equations, where, notably, the dynamical equations for $\mathbf{q}(t)$ are slaved by the solutions for $\mathbf{m}(t)$, as the r.h.s. of Eqs. (S19)-(S21) do not depend on $\mathbf{q}(t)$.

S3.1.1. Difference with respect to mean-field approximation

Finally, let us point out the crucial difference between the mean-field on the one hand and the monomer and BG approximation on the other hand, which lies in the treatment of the averaging of the term $\langle \tanh(\Delta E_i^\mu/2) \rangle$. Whereas the mean-field approximation (uncontrollably) moves the average to the argument, i.e., $\langle \tanh(\Delta E_i^\mu/2) \rangle \approx \tanh(\langle \Delta E_i^\mu/2 \rangle)$, the monomer and BG approximations use the fact that the value of $\Delta E_i^\mu/2$ lies in an enumerable set given by $U_{l,n}^\mu \equiv [2l - z]J_\mu + [2n - 1]K_\mu$ with $l \in \{0, \dots, z\}$ and $n \in \{0, 1\}$. This allows for an explicit summation

$$\langle \tanh(\Delta E_i^\mu/2) \rangle = \sum_{l=0}^z \sum_{n=0}^1 \mathcal{P}_{l,n}^\mu(t) \tanh(U_{l,n}^\mu), \quad (\text{S30})$$

where only the probability $\mathcal{P}_{l,n}^\mu(t)$ is approximated according to Eq. (S27)-(S28) in the monomer approximation.

S3.2. The Bethe-Guggenheim “pair” approximation

In the previous method, we did not take into account nearest-neighbor correlations in the evaluation of $\mathcal{P}_{l,n}^\mu(t)$, which we aim to include in this Section. Let us focus on the probability of picking a spin on the a lattice with a given specific local environment. The same reasoning will also apply for picking a spin on the b lattice. First, we split the probability in a contribution of picking an up or down spin

$$\mathcal{P}_{l,n}^a(t) = \mathcal{P}_{l,n}^{a+}(t) + \mathcal{P}_{l,n}^{a-}(t), \quad (\text{S31})$$

where, e.g., $\mathcal{P}_{l,n}^{a+}(t)$ is the probability of picking an up spin with l neighboring up spins on the a lattice and n neighboring up spins on the b lattice at time t . On the BG level we assume ideal mixing of nearest-neighbor spin pairs, resulting in the following expression

$$\mathcal{P}_{l,n}^{a+} = \underbrace{\left[\frac{N_+^a}{N} \right]}_{\substack{\text{probability} \\ \text{for up spin} \\ \text{on the } a \text{ lattice}}} \times \underbrace{\left[\binom{N_{++}^{aa}}{l} \binom{N_{+-}^{aa}/2}{z-l} / \binom{N_{++}^{aa} + N_{+-}^{aa}/2}{z} \right]}_{\substack{\text{probability for} \\ l \text{ neighboring up} \\ \text{spins on the } a \text{ lattice}}} \times \underbrace{\left[\binom{N_{++}^{ab}}{n} \binom{N_{+-}^{ab}}{1-n} / \binom{N_{++}^{ab} + N_{+-}^{ab}}{1} \right]}_{\substack{\text{probability for} \\ n \text{ neighboring up} \\ \text{spins on the } b \text{ lattice}}}, \quad (\text{S32})$$

$$\mathcal{P}_{l,n}^{a-} = \underbrace{\left[\frac{N_-^a}{N} \right]}_{\substack{\text{probability} \\ \text{for down spin} \\ \text{on the } a \text{ lattice}}} \times \underbrace{\left[\binom{N_{+-}^{aa}/2}{l} \binom{N_{--}^{aa}}{z-l} / \binom{N_{+-}^{aa}/2 + N_{--}^{aa}}{z} \right]}_{\substack{\text{probability for} \\ l \text{ neighboring up} \\ \text{spins on the } a \text{ lattice}}} \times \underbrace{\left[\binom{N_{+-}^{ab}}{n} \binom{N_{--}^{ab}}{1-n} / \binom{N_{+-}^{ab} + N_{--}^{ab}}{1} \right]}_{\substack{\text{probability for} \\ n \text{ neighboring up} \\ \text{spins on the } b \text{ lattice}}}, \quad (\text{S33})$$

where, for example, N_{+-}^{ab} is the total number of nearest-neighbor spin pairs with an up spin on the a lattice and a down spin on the b lattice. To relate N_{+-}^{ab} and the other spin pair numbers to the short- and long-range order, we make use of the following exact relations for periodic lattices

$$2N_{\pm\pm}^{\mu\mu} + N_{+-}^{\mu\mu} = zN_{\pm}^{\mu}, \quad (\text{S34})$$

$$N_{\pm\pm}^{ab} + N_{\pm\mp}^{ab} = N_{\pm}^a, \quad (\text{S35})$$

in combination with Eq. (S25). Furthermore, we use the definition of short-range order (see Eqs. (S8)-(S9)) to write

$$q^{\mu\mu} = 2(N_{++}^{\mu\mu} + N_{--}^{\mu\mu} - N_{+-}^{\mu\mu})/zN = 1 - 4N_{+-}^{\mu\mu}/zN, \quad (\text{S36})$$

$$\begin{aligned} q^{ab} &= (N_{++}^{ab} + N_{--}^{ab} - N_{+-}^{ab} - N_{-+}^{ab})/N \\ &= 1 - 2N_{+-}^{ab}/N - 2N_{-+}^{ab}/N \\ &= 1 + m^a - m^b - 4N_{+-}^{ab}/N, \end{aligned} \quad (\text{S37})$$

where in the last line we used the exact relation

$$m^b - m^a = 2(N_{-+}^{ab} - N_{+-}^{ab})/N. \quad (\text{S38})$$

Using the relations (S34)-(S37) we obtain the following result for the spin pairs within the same lattice

$$N_{\pm\pm}^{\mu\mu} = (z/8)N(1 \pm 2m^\mu + q^{\mu\mu}), \quad (\text{S39})$$

$$N_{\pm\mp}^{\mu\mu} = (z/4)N(1 - q^{\mu\mu}), \quad (\text{S40})$$

and for the spin pairs between the two opposing lattices

$$N_{\pm\pm}^{ab} = (1/4)N(1 \pm m^a \pm m^b + q^{ab}), \quad (\text{S41})$$

$$N_{\pm\mp}^{ab} = (1/4)N(1 \pm m^a \mp m^b - q^{ab}). \quad (\text{S42})$$

Inserting these relations back into Eqs. (S32)-(S33) and taking the thermodynamic limit $N \rightarrow \infty$ while keeping $\mathbf{m}(t)$ and $\mathbf{q}(t)$ fixed, we obtain (omitting, for convenience, arguments on the l.h.s.)

$$\mathcal{P}_{l,n}^{a+}(t) \simeq \frac{C_l^z (1 + 2m^a(t) + q^{aa}(t))^l (1 + m^a(t) - m^b(t) - q^{ab}(t))^{1-n}}{(1 + m^a(t))^z (1 - q^{aa}(t))^{l-z} (1 + m^a(t) + m^b(t) + q^{ab}(t))^{-n}}, \quad (\text{S43})$$

$$\mathcal{P}_{l,n}^{a-}(t) \simeq \frac{C_l^z (1 - 2m^a(t) + q^{aa}(t))^{z-l} (1 - m^a(t) - m^b(t) + q^{ab}(t))^{1-n}}{(1 - m^a(t))^z (1 - q^{aa}(t))^{-l} (1 - m^a(t) + m^b(t) - q^{ab}(t))^{-n}}, \quad (\text{S44})$$

where \mathcal{C}_l^z is given in Eq. (S29). Expressions (S43)-(S44) are given in the main Letter in Eq. (6). The expressions for $\mathcal{P}_{l,n}^{b\pm}(t)$ are similar to Eqs. (S43)-(S44) upon interchanging $m^a(t)$ and $m^b(t)$ and replacing $q^{aa}(t)$ with $q^{bb}(t)$. The difference with the ‘‘monomer’’ approximation (S27) and (S28) is that in the BG approximation the probability also depends explicitly on the short-range order $\mathbf{q}(t)$. Inserting Eqs. (S43)-(S44) into Eq. (S31), and finally into Eqs. (S19)-(S21), leads to a closure of the five coupled non-linear differential equations.

S4. LINEAR STABILITY ANALYSIS

Here, we investigate the stability of steady-states of Eqs. (5) in the Letter, in combination with the aforementioned approximation techniques, using linear stability analysis. This allows us to identify the region in parameter space where we have a so-called Hopf bifurcation, which marks the transition from a (non-oscillatory) steady-state to coherent oscillations.

S4.1. The ‘‘monomer’’ approximation

Since in the MF approximation the short-range order is slaved by the long-range order, it suffices to consider the linear stability analysis for the long-range order. Let us consider a small perturbation of the long-range order around the steady-state value \mathbf{m}_s , i.e., $\mathbf{m}(t) = \mathbf{m}_s + \delta\mathbf{m}(t)$. The most interesting steady-state value to consider is given by the disordered state $\mathbf{m}_s = 0$, in which case the probability (S27)-(S28) can be expanded as

$$\mathcal{P}_{l,n}^a(t) = 2\mathcal{C}_l^z (1 + (2l - z)\delta m^a(t) + (2n - 1)\delta m^b(t)) + \mathcal{O}(\delta\mathbf{m}^2(t)), \quad (\text{S45})$$

$$\mathcal{P}_{l,n}^b(t) = 2\mathcal{C}_l^z (1 + (2l - z)\delta m^b(t) + (2n - 1)\delta m^a(t)) + \mathcal{O}(\delta\mathbf{m}^2(t)). \quad (\text{S46})$$

Inserting this linearized expression back into Eq. (S19), we eventually obtain

$$\tau \frac{d\delta\mathbf{m}(t)}{dt} = \underbrace{\begin{pmatrix} \hat{M}_{aa} & \hat{M}_{ab} \\ \hat{M}_{ba} & \hat{M}_{bb} \end{pmatrix}}_{\mathbb{M}(J,K)} \delta\mathbf{m}(t) + \mathcal{O}(\delta\mathbf{m}^2(t)), \quad (\text{S47})$$

where the entries of the matrix $\hat{\mathbb{M}}$ read

$$\hat{M}_{\mu\mu}(J_\mu, K_\mu) = 2 \sum_{l=0}^z \sum_{n=0}^1 (2l - z) \mathcal{C}_l^z \tanh(U_{l,n}^\mu) - 1, \quad (\text{S48})$$

$$\hat{M}_{ab}(J_a, K_a) = 2 \sum_{l=0}^z \sum_{n=0}^1 (2n - 1) \mathcal{C}_l^z \tanh(U_{l,n}^a), \quad (\text{S49})$$

$$\hat{M}_{ba}(J_b, K_b) = 2 \sum_{l=0}^z \sum_{n=0}^1 (2n - 1) \mathcal{C}_l^z \tanh(U_{l,n}^b). \quad (\text{S50})$$

Note that $\hat{M}_{\mu\mu}$ can be written in terms of the the steady-state solution for the short-range order given by Eq. (S20), i.e., $\hat{M}_{\mu\mu} = zq_s^{\mu\mu} - 1$, which we will make use of in the remaining calculation. Furthermore, the off-diagonals are related to the steady-state of the short-range order between the lattices, i.e., $\hat{M}_{ab} + \hat{M}_{ba} = 2q_s^{ab}$. Hence, a perturbation of the long-range order couples to the steady-state value of the short-range order. The solution of Eq. (S47) can be written in terms of an eigenmode expansion

$$\delta\mathbf{m}(t) = \sum_{k=\pm} \mathcal{A}_k e^{\hat{\lambda}_k t / \tau} \hat{\nu}_k, \quad (\text{S51})$$

where \mathcal{A}_\pm are set by the initial conditions, $\hat{\lambda}_\pm$ are the eigenvalues of the linear stability matrix

$$\hat{\lambda}_\pm = \left(\text{tr}(\hat{\mathbb{M}}) \pm \sqrt{\text{tr}(\hat{\mathbb{M}})^2 - 4\text{det}(\hat{\mathbb{M}})} \right) / 2, \quad (\text{S52})$$

with

$$\text{tr}(\hat{\mathbf{M}}) = z(q_s^{aa} + q_s^{bb}) - 2, \quad (\text{S53})$$

$$\det(\hat{\mathbf{M}}) = (zq_s^{aa} - 1)(zq_s^{bb} - 1) - \hat{M}_{ab}\hat{M}_{ba}, \quad (\text{S54})$$

and the eigenvectors $\hat{\boldsymbol{\nu}}_{\pm}$ read

$$\hat{\boldsymbol{\nu}}_{\pm} = ([\hat{\lambda}_{\pm} + 2(1 - zq_s^{bb})]/\hat{M}_{ba}, 1)^{\text{T}}. \quad (\text{S55})$$

Since all matrix entries in (S47) are real, the characteristic polynomial also has real coefficients. Therefore, if the eigenvalues are complex, they come in complex-conjugate pairs. The perturbation $\delta\mathbf{m}(t)$ grows in time when $\text{Re}(\hat{\lambda}_{\pm}) > 0$, and shrinks in time when $\text{Re}(\hat{\lambda}_{\pm}) < 0$. The imaginary part of the eigenvalues tells us whether the perturbation develops oscillations in time $\text{Im}(\hat{\lambda}_{\pm}) \neq 0$, or is monotonic in time $\text{Im}(\hat{\lambda}_{\pm}) = 0$. The Hopf bifurcation, also known as an oscillatory instability or type-II_o instability in the Cross-Hohenberg classification [3], occurs when the complex conjugate eigenvalues cross the imaginary axis in the complex plane. Based on Eq. (S52), this occurs when

$$\text{tr}(\hat{\mathbf{M}}) = 0 \rightarrow q_s^{aa} + q_s^{bb} = 2/z, \quad (\text{S56})$$

$$\det(\hat{\mathbf{M}}) > 0 \rightarrow (zq_s^{aa} - 1)(zq_s^{bb} - 1) - \hat{M}_{ab}\hat{M}_{ba} > 0. \quad (\text{S57})$$

For fixed z , both equations can be solved explicitly to obtain expressions for the critical values of the parameters J_{μ} and K_{μ} on the line of Hopf bifurcations. Note that Eq. (S56) sets a direct constraint on the steady-state short-range order values.

S4.1.1. Perfectly nonreciprocal setting

Focusing on the perfect nonreciprocal setting with $J_a = J_b = J$ and $K_a = -K_b = K$, we have $q_s^{aa} = q_s^{bb} \equiv q_s(J, K)$ and $\hat{M}_{ab} = -\hat{M}_{ba}$. Under these conditions, Eqs. (S56)-(S57) transform into,

$$\text{tr}(\hat{\mathbf{M}}) = 0 \rightarrow q_s = 1/z, \quad (\text{S58})$$

$$\det(\hat{\mathbf{M}}) > 0 \rightarrow \hat{M}_{ab} \neq 0, \quad (\text{S59})$$

where the latter equation is directly satisfied for $K \neq 0$ (a proof is given in S4.2.2.). Hence, also in the ‘‘monomer’’ expression we find a critical value for the short-range order, which is given by $q_{\text{crit}} \equiv 1/z$. Upon inserting Eq. (S48) into Eq. (S58), one can obtain an explicit result for the Hopf line in the (J, K) -plane.

S4.2. The Bethe-Guggenheim ‘‘pair’’ approximation

In the BG approximation, we can no longer neglect the short-range order for the linear stability analysis. Hence, we consider a small perturbation of the long- and short-range order around their respective steady-state values

$$\mathbf{m}(t) = \mathbf{m}_s + \delta\mathbf{m}(t), \quad (\text{S60})$$

$$\mathbf{q}(t) = \mathbf{q}_s + \delta\mathbf{q}(t). \quad (\text{S61})$$

For the sake of simplicity, we directly focus on the perfectly nonreciprocal setting with $J_a = J_b = J$ and $K_a = -K_b = K$.

S4.2.1. Steady-state short-range order

The trivial steady state is given by the disordered state with $m_s^{\mu} = 0$ and $q_s^{ab} = 0$. To solve for the steady state of the short-range order, denoted as $q_s^{aa} = q_s^{bb} \equiv q_s(J, K)$, we need to solve

$$q_s(J, K) = \frac{1}{z} \sum_{l=0}^z \sum_{n=0}^1 (2l - z)(\overline{\mathcal{P}}_l^+ + \overline{\mathcal{P}}_l^-) \tanh(U_{l,n}^a), \quad (\text{S62})$$

where $\overline{\mathcal{P}}_l^\pm$ are the probabilities (S43)-(S44) evaluated at steady-state values

$$\overline{\mathcal{P}}_l^\pm \equiv \mathcal{C}_l^z (1 \mp q_s)^{z-l} (1 \pm q_s)^l. \quad (\text{S63})$$

Equation (S62) can be solved for specific integer values of z . For example, for $z \in \{2, 3\}$ we obtain

$$q_s(J, K)|_{z=2} = \frac{2 - \sqrt{4 - [\sum_{n=\pm} \tanh(2J + nK)]^2}}{\sum_{n=\pm} \tanh(2J + nK)}, \quad (\text{S64})$$

$$q_s(J, K)|_{z=3} = \frac{4 - \sqrt{16 - \sum_{n=\pm} [\tanh(J+nK) - 3 \tanh(3J+nK)] \sum_{n=\pm} [\tanh(J+nK) + \tanh(3J+nK)]}}{\sum_{n=\pm} [\tanh(J+nK) - 3 \tanh(3J+nK)]}. \quad (\text{S65})$$

For $z = 4$ the solution can be compactly written as the solution to a quartic equation

$$q_s(J, K)|_{z=4} = \mathcal{S}(J, K) - (1/2) \sqrt{-4\mathcal{S}(J, K)^2 + 2\mathcal{H}(J, K) + \mathcal{Q}(J, K)/\mathcal{S}(J, K)}, \quad (\text{S66})$$

where we have introduced the auxiliary functions

$$\mathcal{H}(J, K) \equiv \frac{3 \cosh(4J) [\cosh(4J) + \cosh(2K)]}{\sinh^2(2J) [\cosh(4J) - 2 \sinh^2(K)]}, \quad (\text{S67})$$

$$\mathcal{Q}(J, K) \equiv 16 \left(\sum_{n=\pm} [\tanh(4J + nK) - 2 \tanh(2J + nK)] \right)^{-1}, \quad (\text{S68})$$

$$\mathcal{S}(J, K) \equiv (1/2) \sqrt{(2/3) \mathcal{H}(J, K) + (\mathcal{Q}(J, K)/6) (\mathcal{A}(J, K) + \Delta_0(J, K)/\mathcal{A}(J, K))}, \quad (\text{S69})$$

$$\mathcal{A}(J, K) \equiv 2^{-1/3} \left(\Delta_1(J, K) + \sqrt{\Delta_1^2(J, K) - 4\Delta_0^3(J, K)} \right)^{1/3}, \quad (\text{S70})$$

$$\Delta_0(J, K) \equiv -(3/4) \sum_{n=\pm} [\tanh(2J+nK) + \tanh(4J+nK)] \sum_{n=\pm} [\tanh(2J+nK) - \tanh(4J+nK)], \quad (\text{S71})$$

$$\Delta_1(J, K) \equiv 216 \cosh(2J) \cosh(2K) \operatorname{sech}(4J-K) \operatorname{sech}(4J+K) \sinh^3(2J) \sinh^2(K) [\cosh(4J) + \cosh(2K)]^{-2}. \quad (\text{S72})$$

Upon inserting the steady-state values, the probability can be expanded up to first order in $\delta \mathbf{m}(t)$ and $\delta \mathbf{q}(t)$, which reduces Eqs. (5) in the main Letter to the following linear set of equations

$$\tau \frac{d}{dt} \begin{pmatrix} \delta \mathbf{m}(t) \\ \delta \mathbf{q}(t) \end{pmatrix} = \begin{pmatrix} \mathbf{M} & \mathbf{0} \\ \mathbf{0} & \mathbf{Q} \end{pmatrix} \begin{pmatrix} \delta \mathbf{m}(t) \\ \delta \mathbf{q}(t) \end{pmatrix}, \quad (\text{S73})$$

where $\mathbf{M}(J, K)$ is a 2×2 matrix and $\mathbf{Q}(J, K)$ a 3×3 matrix. Due to the diagonal block structure of the linearized equations, we can handle the perturbations for $\delta \mathbf{m}(t)$ and $\delta \mathbf{q}(t)$ separately.

S4.2.2. Linear stability of long-range order

The elements of the 2×2 matrix \mathbf{M} are given by

$$M_{aa}(J, K) = M_{bb}(J, K) = \frac{q_s/q_{\text{crit}} - 1}{1 + q_s} \left[1 - 2 \sum_{l=0}^z \sum_{n=0}^1 \overline{\mathcal{P}}_l^+ \tanh(U_{l,n}^a) \right], \quad (\text{S74})$$

$$M_{ab}(J, K) = -M_{ba}(J, K) = \sum_{l=0}^z \sum_{n=0}^1 (2n-1) (\overline{\mathcal{P}}_l^+ + \overline{\mathcal{P}}_l^-) \tanh(U_{l,n}^a), \quad (\text{S75})$$

where $q_{\text{crit}} \equiv 1/(z-1)$. Note that Eqs. (S74)-(S75) are equivalent to Eqs. (7) in the Letter. Further analysis regarding the solution for $\delta \mathbf{m}(t)$ is given in the Letter. Here, we are left to prove that $M_{ab}(J, K \neq 0) \neq 0$. To see this, let us explicitly write out the first sum over n

$$M_{ab} = \sum_{l=0}^z \sum_{n=0}^1 (2n-1) (\overline{\mathcal{P}}_l^+ + \overline{\mathcal{P}}_l^-) \tanh(U_{l,n}^a) = \sum_{l=0}^z (\overline{\mathcal{P}}_l^+ + \overline{\mathcal{P}}_l^-) (\tanh([2l-z]J+K) - \tanh([2l-z]J-K)), \quad (\text{S76})$$

Note that $\overline{\mathcal{P}}_l^\pm \geq 0$ for $q_s \in [-1, 1]$, which follows straightforwardly from Eq. (S63). Furthermore, since $\tanh(x)$ is an increasing function of x , we have $\tanh([2l-z]J+K) - \tanh([2l-z]J-K) > 0$ for $K > 0$ and $\tanh([2l-z]J+K) - \tanh([2l-z]J-K) < 0$ for $K < 0$. Hence, M_{ab} is given by a sum over strictly positive (for $K > 0$) or negative (for $K < 0$) terms, rendering $M_{ab} \neq 0$ for $K \neq 0$. This outcome results in complex eigenvalues for \mathbf{M} , as explained in the Letter.

S4.2.3. Linear stability of short-range order

The elements of the 3×3 matrix \mathbf{Q} are given by

$$Q_{11} = Q_{22} = -2 - \frac{2zq_s^2}{1-q_s^2} + \frac{2/z}{1-q_s^2} \sum_{l=0}^z \sum_{n=0}^1 (2l-z)^2 (\overline{\mathcal{P}}_l^+ - \overline{\mathcal{P}}_l^-) \tanh(U_{l,n}^a), \quad (\text{S77})$$

$$Q_{12} = Q_{21} = 0, \quad (\text{S78})$$

$$Q_{13} = -Q_{23} = \frac{2}{z} \sum_{l=0}^z \sum_{n=0}^1 (2l-z)(2n-1) (\overline{\mathcal{P}}_l^+ - \overline{\mathcal{P}}_l^-) \tanh(U_{l,n}^a), \quad (\text{S79})$$

$$Q_{31} = -Q_{32} = \frac{1}{1-q_s^2} \sum_{l=0}^z \sum_{n=0}^1 (2n-1) [(2l-z)(\overline{\mathcal{P}}_l^+ - \overline{\mathcal{P}}_l^-) - zq_s(\overline{\mathcal{P}}_l^+ + \overline{\mathcal{P}}_l^-)] \tanh(U_{l,n}^a), \quad (\text{S80})$$

$$Q_{33} = -2 + \sum_{\mu} \sum_{l=0}^z \sum_{n=0}^1 (\overline{\mathcal{P}}_l^+ - \overline{\mathcal{P}}_l^-) \tanh(U_{l,n}^\mu). \quad (\text{S81})$$

The solution of the linearized equation for $\delta\mathbf{q}(t)$ reads

$$\delta\mathbf{q}(t) = \sum_{i=1}^3 \mathcal{A}_i e^{\tilde{\lambda}_i t / \tau} \tilde{\mathbf{v}}_i, \quad (\text{S82})$$

where the \mathcal{A}_i are determined by the initial conditions, and the eigenvalues of \mathbf{Q} , denoted as $\tilde{\lambda}_i$, are given by

$$\tilde{\lambda}_1 = Q_{11}, \quad (\text{S83})$$

$$\tilde{\lambda}_2 = \frac{1}{2} \left(Q_{11} + Q_{33} + \sqrt{8Q_{13}Q_{31} + (Q_{11} - Q_{33})^2} \right), \quad (\text{S84})$$

$$\tilde{\lambda}_3 = \frac{1}{2} \left(Q_{11} + Q_{33} - \sqrt{8Q_{13}Q_{31} + (Q_{11} - Q_{33})^2} \right), \quad (\text{S85})$$

and finally, the eigenvectors of \mathbf{Q} , denoted as $\tilde{\mathbf{v}}_i$, read

$$\tilde{\mathbf{v}}_1 = (1, 1, 0)^T, \quad (\text{S86})$$

$$\tilde{\mathbf{v}}_2 = (-Q_{13}/(\tilde{\lambda}_2 - Q_{33}), Q_{13}/(\tilde{\lambda}_2 - Q_{33}), 1)^T, \quad (\text{S87})$$

$$\tilde{\mathbf{v}}_3 = (-Q_{13}/(\tilde{\lambda}_3 - Q_{33}), Q_{13}/(\tilde{\lambda}_3 - Q_{33}), 1)^T. \quad (\text{S88})$$

Note that $\tilde{\lambda}_1$ is always real, and therefore cannot give rise to a Hopf bifurcation. The second and third eigenvalues can become complex, in which case their real part is given by $\text{Re}(\tilde{\lambda}_{2,3}) = (Q_{11} + Q_{33})/2$. However, we now prove that $Q_{11} \leq 0$ and $Q_{33} \leq 0$, and therefore also $\tilde{\lambda}_{2,3}$ cannot give rise to a Hopf bifurcation.

To prove that $Q_{11} \leq 0$ we proceed with the following chain of inequalities

$$\begin{aligned}
Q_{11} &= -2 - \frac{2zq_s^2}{1-q_s^2} + \frac{2/z}{1-q_s^2} \sum_{l=0}^z \sum_{n=0}^1 (2l-z)^2 (\overline{\mathcal{P}}_l^+ - \overline{\mathcal{P}}_l^-) \tanh(U_{l,n}^a) \\
&\leq -2 - \frac{2zq_s^2}{1-q_s^2} + \left| \frac{2/z}{1-q_s^2} \sum_{l=0}^z \sum_{n=0}^1 (2l-z)^2 (\overline{\mathcal{P}}_l^+ - \overline{\mathcal{P}}_l^-) \tanh(U_{l,n}^a) \right| \\
&\leq -2 - \frac{2zq_s^2}{1-q_s^2} + \frac{2/z}{1-q_s^2} \sum_{l=0}^z \sum_{n=0}^1 |(2l-z)^2 (\overline{\mathcal{P}}_l^+ - \overline{\mathcal{P}}_l^-) \tanh(U_{l,n}^a)| \\
&\leq -2 - \frac{2zq_s^2}{1-q_s^2} + \frac{2/z}{1-q_s^2} \sum_{l=0}^z |(2l-z)^2 (\overline{\mathcal{P}}_l^+ - \overline{\mathcal{P}}_l^-)| |\tanh([2l-z]J+K) + \tanh([2l-z]J-K)| \\
&\leq -2 - \frac{2zq_s^2}{1-q_s^2} + \frac{4/z}{1-q_s^2} \sum_{l=0}^z (2l-z)^2 |\overline{\mathcal{P}}_l^+ - \overline{\mathcal{P}}_l^-| \\
&\leq -2 - \frac{2zq_s^2}{1-q_s^2} + \frac{4/z}{1-q_s^2} \sum_{l=0}^z (2l-z)^2 (\overline{\mathcal{P}}_l^+ + \overline{\mathcal{P}}_l^-) = 0,
\end{aligned} \tag{S89}$$

where the last inequality follows from the triangle inequality $|\overline{\mathcal{P}}_l^+ - \overline{\mathcal{P}}_l^-| \leq |\overline{\mathcal{P}}_l^+| + |\overline{\mathcal{P}}_l^-|$ together with $\overline{\mathcal{P}}_l^\pm \geq 0$ and therefore $|\overline{\mathcal{P}}_l^\pm| = \overline{\mathcal{P}}_l^\pm$. Next, we proceed with Q_{33} in a similar fashion

$$\begin{aligned}
Q_{33} &= -2 + \sum_{\mu} \sum_{l=0}^z \sum_{n=0}^1 (\overline{\mathcal{P}}_l^+ - \overline{\mathcal{P}}_l^-) \tanh(U_{l,n}^\mu) \\
&= -2 + 2 \sum_{l=0}^z (\overline{\mathcal{P}}_l^+ - \overline{\mathcal{P}}_l^-) [\tanh([2l-z]J+K) + \tanh([2l-z]J-K)] \\
&\leq -2 + \left| 2 \sum_{l=0}^z (\overline{\mathcal{P}}_l^+ - \overline{\mathcal{P}}_l^-) [\tanh([2l-z]J+K) + \tanh([2l-z]J-K)] \right| \\
&\leq -2 + 2 \sum_{l=0}^z \left| (\overline{\mathcal{P}}_l^+ - \overline{\mathcal{P}}_l^-) [\tanh([2l-z]J+K) + \tanh([2l-z]J-K)] \right| \\
&\leq -2 + 4 \sum_{l=0}^z |\overline{\mathcal{P}}_l^+ - \overline{\mathcal{P}}_l^-| \\
&\leq -2 + 4 \sum_{l=0}^z (\overline{\mathcal{P}}_l^+ + \overline{\mathcal{P}}_l^-) = -2 + 2 = 0,
\end{aligned} \tag{S90}$$

where for the last inequality we again used the triangle inequality. This establishes that $Q_{11} \leq 0$ and $Q_{33} \leq 0$, and therefore when $\tilde{\lambda}_{2,3}$ become complex, their real part obeys the bound $\text{Re}(\tilde{\lambda}_{2,3}) = (Q_{11} + Q_{33})/2 \leq 0$. Hence, up to first order, any perturbation $\delta \mathbf{q}(t)$ decays over time. The *coherent oscillations in $\mathbf{q}(t)$* observed in Fig. 1c,d in the main Letter *are therefore an inherently nonlinear effect* related to the coupling between $\mathbf{m}(t)$ and $\mathbf{q}(t)$.

S5. DIVERGENCE OF THE RESIDENCE TIME UPON APPROACHING THE SNIPER BIFURCATION

Consider the perfectly nonreciprocal setting with $J_a = J_b = J$ and $K_a = -K_b = K$. Figure 2c in the main Letter shows the magnetization oscillating between 4 ghost states upon approaching the degenerate saddle-node-infinite-period (SNIPER) bifurcation from below, i.e. $J \uparrow J_{\text{SNP}}(K)$, where $J_{\text{SNP}}(K)$ is the J value of the SNIPER bifurcation for a given nonreciprocal coupling K . The residence time \mathcal{T} in the vicinity of these ghost states diverges at the SNIPER bifurcation as (see also Eq. (9) in the main Letter)

$$\mathcal{T} \propto (J_{\text{SNP}}(K) - J)^{-1/2}, \tag{S91}$$

which is shown explicitly in Fig. S1. To see the precise algebraic scaling, we plot $1/\mathcal{T}^2$ against $J_{\text{SNP}}(K) - J$ in Fig. S1b, where we indeed observe very good agreement with the expected scaling (black dashed line) close to the SNIPER bifurcation.

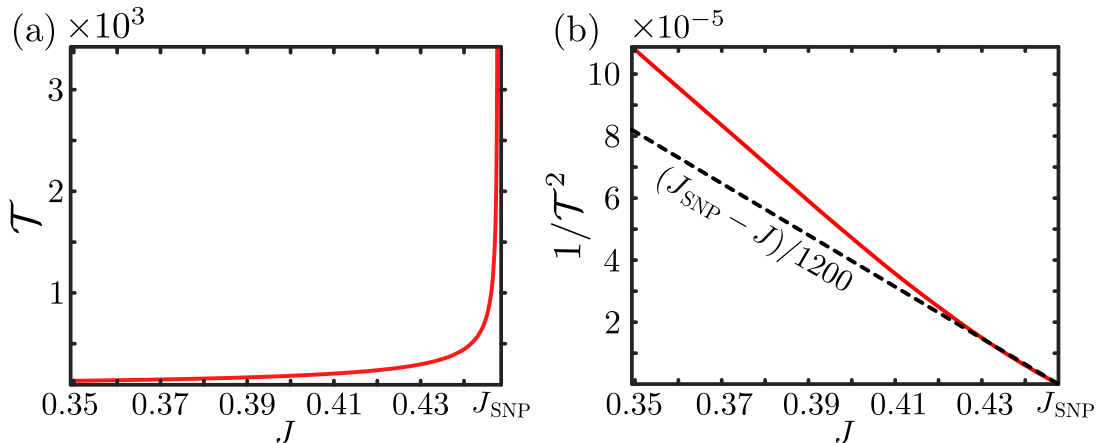


FIG. S1. Algebraic divergence of the residence time \mathcal{T} within a ghost state close to the degenerate saddle-node-infinite-period (SNIPER) bifurcation. Approaching the SNIPER bifurcation from below, the residence time scales as $\mathcal{T} \propto (J_{\text{SNP}}(K) - J)^{-1/2}$, where $J_{\text{SNP}}(K)$ is the J value of the SNIPER bifurcation for a given nonreciprocal coupling K . In both panels we consider $K = 0.1$ and $z = 4$, for which $J_{\text{SNP}} \approx 0.4477$. Results are obtained with the numerical continuation package MATCONT [4].

S6. PROOF OF EXISTENCE OF STATIC LONG-RANGE ORDER ON THE SQUARE LATTICE

In [1] it is claimed that for the perfect nonreciprocal setting with $J_a = J_b = J$ and $K_a = -K_b = K$, any nonzero nonreciprocal coupling $K \neq 0$ destroys the static long-range order in the two-dimensional square-lattice Ising model. The authors’ reasoning behind this claim goes as follows: Consider the low temperature limit, and suppose all spins for the two lattices are either up or down. Then, the total “energy” in both lattices can be written as

$$E^a = -J \sum_{\langle ij \rangle} \sigma_i^a \sigma_j^a - KN, \quad (\text{S92})$$

$$E^b = -J \sum_{\langle ij \rangle} \sigma_i^b \sigma_j^b + KN. \quad (\text{S93})$$

Clearly, lattice b is in a meta-stable state, and therefore tries to flip all spins, thereby transiting to the global minimum. But if this happens, lattice a is in a meta-stable state, and therefore all spins in lattice a try to flip to reach the global minimum. This results in a repetitive cycle of consecutive magnetization reversal in both lattices, thereby destroying the static-order.

One should immediately note, however, that this reasoning is *not* restricted to the square lattice, but also to any other lattice (incl. the fully-connected mean-field lattice), which would indicate that static long-range order is destroyed for any lattice. This is clearly not the case, as the authors themselves show in [1] for the mean field lattice, and we show in the present Letter also for the Bethe lattice. Furthermore, the above argumentation based on gradient descent in the “energy” landscape does *not* apply to a non-equilibrium, detailed-balance violating dynamics.

To resolve this obvious inconsistency, *we prove that static long-range order in the square lattice nonreciprocal Ising model persists upon small perturbations in the nonreciprocal coupling strength.* Thereby, we directly disprove that static-order vanishes in the two-dimensional nonreciprocal Ising model with $K \neq 0$ as stated in [1].

S6.1. Recap of the long-range order

For completeness, we recall some statements about the long-range order. We define the long-range order in lattice a and b as (see also Eq. (S7); here we explicitly write out the averaging $\langle \cdot \rangle$)

$$m^\mu(t) \equiv N^{-1} \sum_{\{\sigma\}} \sum_{i=1}^N \sigma_i^\mu P(\sigma; t), \quad (\text{S94})$$

where $\{\boldsymbol{\sigma}\}$ denotes the set of all possible spin configurations $\boldsymbol{\sigma}$. From the master equation (S2) we can obtain the time-evolution equation for the magnetization [2]

$$\frac{dm^\mu(t)}{dt} = -2N^{-1} \sum_{\{\boldsymbol{\sigma}\}} \sum_{i=1}^N \sigma_i^\mu w_i^\mu(\sigma_i^\mu) P(\boldsymbol{\sigma}; t). \quad (\text{S95})$$

In the steady-state we have $dm^\mu(t)/dt = 0$, and therefore

$$\sum_{\{\boldsymbol{\sigma}\}} \sum_{i=1}^N \sigma_i^\mu w_i^\mu(\sigma_i^\mu) P_s(\boldsymbol{\sigma}) = 0, \quad (\text{S96})$$

where $P_s(\boldsymbol{\sigma}) \equiv \lim_{t \rightarrow \infty} P(\boldsymbol{\sigma}; t)$ denotes the steady-state probability.

S6.2. Steady-state for $K = 0$

Let us first recall the steady-state long-range order for $K = 0$, where we have two independent Ising systems on lattice a and b , respectively. Let $P_{0,s}(\boldsymbol{\sigma})$ and $w_{0,i}^\mu(\sigma_i^\mu)$ be the steady-state probability and transition rate when $K = 0$, respectively. Note that $\sum_{\{\boldsymbol{\sigma}\}} P_{0,s}(\boldsymbol{\sigma}) = 1$. The steady-state long-range order for $K = 0$, denoted as $m_{0,s}^\mu$, reads [5]

$$m_{0,s}^\mu \equiv N^{-1} \sum_{\{\boldsymbol{\sigma}\}} \sum_{i=1}^N \sigma_i^\mu P_{0,s}(\boldsymbol{\sigma}) = \pm (1 - \sinh^{-4}(2J))^{1/8}, \quad (\text{S97})$$

which is nonzero for $J > \ln(1 + \sqrt{2})/2$.

S6.3. Perturbation expansion in K

We consider a perturbation of the steady-state under a small change in K such that $|K| \ll 1$. For small perturbations we can expand the transition rates as follows,

$$w_i^\mu(\sigma_i^\mu) = w_{0,i}^\mu(\sigma_i^\mu) + K \delta w_i^\mu(\sigma_i^\mu) + \mathcal{O}(K^2), \quad (\text{S98})$$

where it follows from a Taylor expansion of Eq. (S3) that

$$\delta w_i^\mu(\sigma_i^\mu) = (1/2\tau)[1 - 2\delta_{\mu,b}]\sigma_i^a \sigma_i^b \operatorname{sech}^2(J \sum_{\langle i|j \rangle} \sigma_j^\mu), \quad (\text{S99})$$

with $\delta_{\mu,b} = 1$ when $\mu = b$ and $\delta_{\mu,b} = 0$ when $\mu = a$. A small perturbation in the transition rates induces a perturbation in the steady-state probability

$$P_s(\boldsymbol{\sigma}) = P_{0,s}(\boldsymbol{\sigma}) + K \delta P_s(\boldsymbol{\sigma}) + \mathcal{O}(K^2), \quad (\text{S100})$$

which in turn results in a perturbation of the magnetization, $m_s^\mu = m_{0,s}^\mu + K \delta m_s^\mu + \mathcal{O}(K^2)$, where it follows from Eq. (S97) that

$$\delta m_s^\mu \equiv N^{-1} \sum_{\{\boldsymbol{\sigma}\}} \sum_{i=1}^N \sigma_i^\mu \delta P_s(\boldsymbol{\sigma}). \quad (\text{S101})$$

Our aim is to provide an upper and lower bound for δm_s^μ .

S6.4. Bound on perturbations of long-range order

We start with an upper bound for δm_s^μ , which goes as follows:

$$\begin{aligned}
\delta m_s^\mu &\leq |N^{-1} \sum_{\{\boldsymbol{\sigma}\}} \sum_{i=1}^N \sigma_i^\mu \delta P_s(\boldsymbol{\sigma})| \\
&\leq N^{-1} \sum_{\{\boldsymbol{\sigma}\}} \sum_{i=1}^N |\sigma_i^\mu \delta P_s(\boldsymbol{\sigma})| \\
&= N^{-1} \sum_{\{\boldsymbol{\sigma}\}} \sum_{i=1}^N |\sigma_i^\mu| |\delta P_s(\boldsymbol{\sigma})| \\
&= \sum_{\{\boldsymbol{\sigma}\}} |\delta P_s(\boldsymbol{\sigma})|.
\end{aligned} \tag{S102}$$

In exactly the same way, we can also provide a lower bound

$$\begin{aligned}
\delta m_s^\mu &\geq -|N^{-1} \sum_{\{\boldsymbol{\sigma}\}} \sum_{i=1}^N \sigma_i^\mu \delta P_s(\boldsymbol{\sigma})| \\
&\geq -N^{-1} \sum_{\{\boldsymbol{\sigma}\}} \sum_{i=1}^N |\sigma_i^\mu \delta P_s(\boldsymbol{\sigma})| \\
&= -N^{-1} \sum_{\{\boldsymbol{\sigma}\}} \sum_{i=1}^N |\sigma_i^\mu| |\delta P_s(\boldsymbol{\sigma})| \\
&= -\sum_{\{\boldsymbol{\sigma}\}} |\delta P_s(\boldsymbol{\sigma})|
\end{aligned} \tag{S103}$$

Hence, combining the upper and lower bound, we obtain

$$|\delta m_s^\mu| \leq \sum_{\{\boldsymbol{\sigma}\}} |\delta P_s(\boldsymbol{\sigma})|. \tag{S104}$$

This is our first main result. We are left with determining an upper bound for $\sum_{\{\boldsymbol{\sigma}\}} |\delta P_s(\boldsymbol{\sigma})|$, for which we use the following theorem shown in [6] (Theorem 2.1):

Theorem 1 *Let the Markov chain $X(t)$ with infinitesimal generator \mathbf{A} , i.e., $d\mathbf{p}(t)/dt = \mathbf{p}(t)\mathbf{A}$, be exponentially weakly ergodic; that is, for any normalized initial conditions $\mathbf{p}(t=0)$, and $\mathbf{p}^\dagger(t=0)$, and any $t \geq 0$, there exists a $b > 0$ and $c > 2$ such that*

$$\|\mathbf{p}(t) - \mathbf{p}^\dagger(t)\| \leq ce^{-bt}, \quad t \geq 0, \tag{S105}$$

where $\|\mathbf{p}\| = \sum_i |p_i|$ denotes the l_1 -norm for vectors. Then, for perturbations to the infinitesimal generator, $\mathbf{A} + \hat{\mathbf{A}}$, the following bound takes place for the perturbed stationary probabilities $\hat{\mathbf{p}}_s$:

$$\|\mathbf{p}_s - \hat{\mathbf{p}}_s\| \leq \frac{1 + \ln(c/2)}{b} \|\hat{\mathbf{A}}\|, \tag{S106}$$

where $\|\hat{\mathbf{A}}\| = \max_i \sum_j |\hat{A}_{ij}|$ is the subordinate norm for the perturbation matrix.

Since it is known that (infinite volume) Glauber dynamics on \mathbb{Z}^d is exponentially weakly ergodic (see Theorem 3.3 on page 117 in [7]), we can directly use Theorem 1. To translate the results from Theorem 1 into a bound for $|\delta m_s^\mu|$, we first want to bound the subordinate norm for the perturbed infinitesimal generator. To do so, note that the perturbation to the transition rates obeys the following bound,

$$|K \delta w_i^\mu(\sigma_i^\mu)| = |(K/2\tau)[1 - 2\delta_{\mu,b}]\sigma_i^a \sigma_i^b \operatorname{sech}^2(J \sum_{\langle i|j \rangle} \sigma_j^\mu)| \leq |K/2\tau| = |K|/4N, \tag{S107}$$

where we used that $|\operatorname{sech}^2(x)| \leq 1$ for $x \in \mathbb{R}$ and $\tau \equiv 2N$. These perturbations enter the off-diagonal terms of $\hat{\mathbf{A}}$, so we have established that $\hat{A}_{ij} \leq |K|/4N$ for $i \neq j$. Since we consider single spin-flip dynamics, each row/column in $\hat{\mathbf{A}}$ has $2N$ nonzero entries excluding the diagonal entry, which is equal to $\hat{A}_{ii} = -\sum_j \hat{A}_{ij}$. Therefore, the diagonal term can also be bounded by $|\hat{A}_{ii}| \leq 2N \times |K|/4N$. Combining these results, we obtain the following bound for the subordinate norm of the perturbed infinitesimal generator,

$$\|\hat{\mathbf{A}}\| \leq 2 \times (2N) \times |K|/4N = |K|. \quad (\text{S108})$$

Note, that this result is independent of the system size N . Finally, we note that $\|\mathbf{p}_s - \hat{\mathbf{p}}_s\|$ in Theorem 1 translates into $|K| \sum_{\{\sigma\}} |\delta P_s(\sigma)|$ in our work. Combining all together, we obtain that there exists $b > 0$ and $c > 2$ such that for $K \neq 0$

$$\sum_{\{\sigma\}} |\delta P_s(\sigma)| \leq \frac{1 + \ln(c/2)}{b} < \infty, \quad (\text{S109})$$

and therefore the perturbation is bounded by a finite number independent of K up to first order

$$|\delta m_s^\mu| \leq \frac{1 + \ln(c/2)}{b} < \infty. \quad (\text{S110})$$

S6.5. Connecting the dots and final remark

We have shown that up to first order the static long-range order can be written as $m_s^\mu = m_{0,s}^\mu + K\delta m_s^\mu + \mathcal{O}(K^2)$ under a small perturbation in K , where $m_{0,s}^\mu \neq 0$ for $J > \ln(1 + \sqrt{2})/2$ as shown in Eq. (S97). Furthermore, the perturbation δm_s^μ is bounded by a finite number independent of K , as shown in Eq. (S110). This means that for arbitrary small nonzero K , the perturbed long-range order gets arbitrarily close to the unperturbed value, i.e.

$$|m_s^\mu - m_{0,s}^\mu| \leq |K| \left(\frac{1 + \ln(c/2)}{b} \right). \quad (\text{S111})$$

If the static long-range order vanished for any arbitrary nonzero K on the square lattice, it would indicate that m_s^μ is a discontinuous and non-differentiable function of K for $J > \ln(1 + \sqrt{2})/2$, as it would suddenly jump from $m_{0,s}^\mu \neq 0$ to $m_s^\mu = 0$ in the limit $K \rightarrow 0^+$. This cannot be true, since we have established that m_s^μ gets arbitrarily close to $m_{0,s}^\mu$ up to first order in K . This invalidates the statement that static long-range order is destroyed in the perfectly nonreciprocal Ising model for any $K \neq 0$.

Note that our proof does not state anything about the regime with coherent steady-state oscillations on the square lattice. Similar to the results in [1], we also observe that spiral defects can destroy coherent steady-state oscillations on the square lattice. This, however, does not have any implication for the regime with static order, which is our main focus in this Section.

S7. KINETIC MONTE-CARLO SIMULATIONS

For the results shown in Fig. 1c,d (black dashed lines) and Fig. 3 in the Letter we performed kinetic MC simulations on three different types of lattices: (i) the fully-connected mean field (MF) lattice, (ii) the Bethe lattice, and (iii) the square lattice with periodic boundary conditions. Simulations on the Bethe lattice were performed using the random graph algorithm [8, 9], which works as follows: Let us consider a Bethe lattice with coordination number z . First, we create a Cayley tree of $i = \{1, \dots, N\}$ spins with coordination number z . The spins on the outer layer are only connected to one spin on the inner layer. To create the remaining $z - 1$ connections, we randomly pair spins on the outer layer to other spins on the outer layer. The final result is a Cayley tree with random connections on the outer layer. Note that for both lattices a and b we create new random connections. For large N it has been shown that the Ising model on an ensemble of such random graphs is equivalent to the Ising model on a Bethe lattice [8]. Indeed, for large N we find perfect agreement between the simulations and our theory, as shown in Fig. 1c,d in the main Letter. For the MF lattice, we connect all spins with each other, resulting in a fully connected graph.

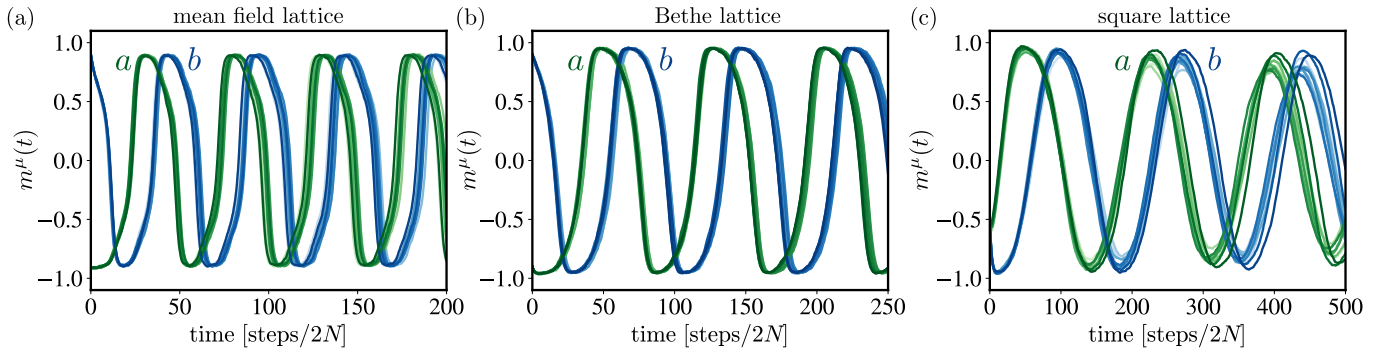


FIG. S2. Oscillations in the long-range order $m^\mu(t)$ on the mean-field lattice (a), Bethe lattice (b), and square lattice (c), obtained by Monte-Carlo simulations. In each panel, we plot 10 independent trajectories for the magnetization on lattice a (green) and b (blue). Fluctuations between the trajectories lead to small differences over time, which are decreasing with increasing system size, a signature of self-averaging. The values for J and K for each of the lattices are reported in table S1.

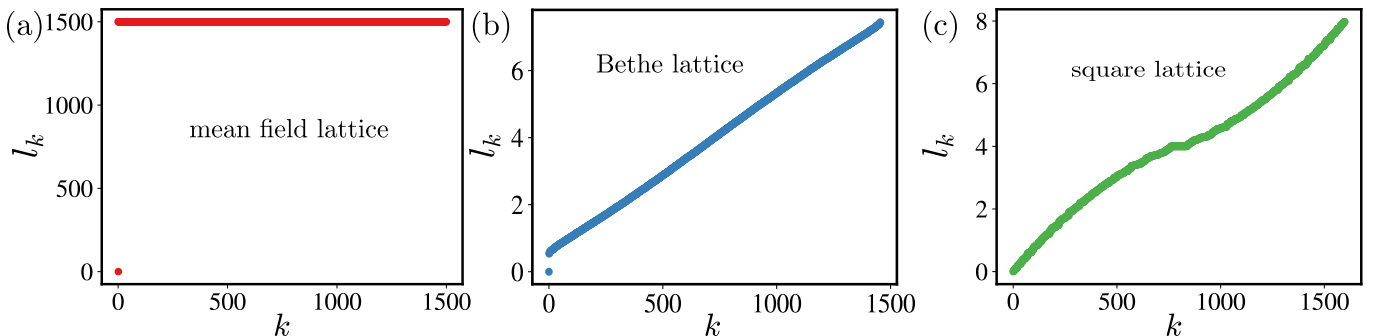


FIG. S3. Eigenvalues l_k of the Laplacian matrix \mathbf{L} for the mean-field lattice (a), Bethe lattice (b), and square lattice (c). For the mean-field lattice, all eigenvalues except for the first are degenerate with value $l_2 = \dots = l_N = N$, where N is the system size given in table S1. The Bethe lattice has a spectral gap between the lowest eigenvalue l_1 and l_2 .

S7.1. Simulation setup

In Table S1 we summarize the system size, number of trajectories, and parameter settings, which were used to obtain the spectral density shown in Fig. 3 in the Letter. As initial conditions, we selected a randomly mixed configuration of up and down spins for fixed magnetization. A subset of trajectories for the short-range order are displayed in Fig. S2, and in each of the lattices we observe coherent oscillations.

TABLE S1. Simulation parameters for results shown in Fig. 3 in the main Letter.

lattice	size (N)	MC steps	# trajectories	J [$k_B T$]	K [$k_B T$]
mean field	1500	1500×10^3	500	$1.5/N$	0.3
Bethe	1457	1457×10^3	500	0.5	0.3
square	40×40	1600×10^3	500	0.6	0.3

To obtain the results shown in Fig. 1c,d we used a Bethe lattice with system size $N = 118097$. Such a large system size was not feasible for the setup of Fig. 3 since the spectral density $\langle |\hat{\Psi}_k^\mu(\omega)| \rangle$ must be averaged over many independent trajectories, resulting in memory issues for too large N .

S7.2. Eigenvalues of Laplacian matrix

In Fig. 3 in the main Letter we plot the spectral density $\langle |\hat{\Psi}_k^\mu(\omega)| \rangle$ as a function of the eigenvalues l_k of the Laplacian matrix \mathbf{L} . To obtain the eigenvalues, we numerically diagonalized the Laplacian \mathbf{L} in Python, and the

resulting eigenvalues are shown in Fig. S3. Note that for the mean-field lattices all eigenvalues except for the first are degenerate and equal to $l_2 = \dots = l_N = N$.

-
- [1] Y. Avni, M. Fruchart, D. Martin, D. Seara, and V. Vitelli, “The non-reciprocal ising model,” (2023), [arXiv:2311.05471](#) [[cond-mat.stat-mech](#)].
 - [2] R. J. Glauber, *J. Math. Phys.* **4**, 294 (1963).
 - [3] M. C. Cross and P. C. Hohenberg, *Rev. Mod. Phys.* **65**, 851 (1993).
 - [4] A. Dhooge, W. Govaerts, and Y. A. Kuznetsov, *ACM Trans. Math. Softw.* **29**, 141–164 (2003).
 - [5] C. N. Yang, *Phys. Rev.* **85**, 808 (1952).
 - [6] A. Y. Mitrophanov, *Journal of Applied Probability* **40**, 970–979 (2003).
 - [7] J. Bertoin, F. Martinelli, and Y. Peres, *Lectures on Probability Theory and Statistics: Ecole d’Ete de Probabilites de Saint-Flour XXVII-1997* (Springer, Berlin Heidelberg, Germany, 2004).
 - [8] D. A. Johnston and P. Plecháč, *J. Phys. A: Math. Gen.* **31**, 475 (1998).
 - [9] D. Dhar, P. Shukla, and J. P. Sethna, *J. Phys. A: Math. Gen.* **30**, 5259 (1997).